BSGF - Earth Sciences Bulletin 2020, 191, 10
© A. El Bakili *et al.*, Published by EDP Sciences 2020
https://doi.org/10.1051/bsgf/2020008

BSGF
Earth Sciences Bulletin
Available online at:
www.bsgf.fr

Neogene polyphase deformation related to the Alboran Basin evolution: new insights for the Beni Bousera massif (Internal Rif, Morocco)

Asmae El Bakili[1,2,*], Michel Corsini[1], Ahmed Chalouan[2], Philippe Münch[3], Adrien Romagny[5], Jean Marc Lardeaux[1,4] and Ali Azdimousa[6]

[1] Université Côte d'Azur, CNRS, Observatoire de la Côte d'Azur, IRD, Géoazur, 250, rue Albert Einstein, 06560 Sophia Antipolis, France
[2] Université Mohammed V, Faculté des Sciences Rabat, 4, avenue Ibn Batouta, B.P. 1014 Rabat, Maroc
[3] Université Montpellier 2, Géosciences Montpellier, UMR 5243, CC 060, place Eugène Bataillon, 34095 Montpellier cedex 5, France
[4] Centre for Lithospheric Research, Czech Geological Survey, Klárov 3, 118 21 Prague 1, Czech Republic
[5] 4, rue du Lavoir, 06340 Drap, France
[6] Université Mohammed premier, Faculté des Sciences, BV Mohammed VI– BP 717, 60000 Oujda, Maroc

Received: 5 September 2019 / Accepted: 6 March 2020

Abstract – Located in the Internal domain of the Rif belt, the Beni Bousera massif is characterized by a stack of peridotites and crustal metamorphic units. The massif is intruded by granitic dykes and affected by several normal ductile shear zones. Structural, petrological and ^{40}Ar–^{39}Ar dating analyses performed on these two elements highlight that (1) the granitic dykes are emplaced within major N70° to N140° trending normal faults and shear zones, resulted from an NNE-SSW extension (2) the Aaraben fault in its NE part is characterized by N70° to N150° trending ductile normal shear zones, resulted from a nearly N-S extension and (3) the age of this extensional event is comprised between 22 and 20 Ma. Available paleomagnetic data allow a restoration of the initial orientation of extension, which was nearly E-W contemporary with the Alboran Basin opening in back-arc context, during the Early Miocene. At the onset of the extension, the peridotites were somehow lying upon a partially melted continental crust, and exhumed during this event by the Aaraben Normal Shear Zone. Afterward, the Alboran Domain suffered several compressional events.

Keywords: Gibraltar arc / peridotites / granitic dykes / ductile shear zones / ^{40}Ar–^{39}Ar dating / back-arc extension

Résumé – Déformation polyphasée néogène liée à l'évolution du bassin d'Alboran : nouvelles données sur le massif de Beni Bousera (Rif interne, Maroc). Dans le Rif interne (domaine d'Alboran), le massif de Beni Bousera expose un empilement de péridotites et d'unités métamorphiques crustales. Ce massif est recoupé par des filons granitiques et affecté par plusieurs zones de cisaillement ductiles normales. Des analyses structurales, pétrologiques et des datations ^{40}Ar–^{39}Ar réalisées sur ces deux types d'objets montrent que, (1) les filons granitiques se sont mis en place dans des zones de failles et des zones de cisaillement normales, orientées en majorité entre N70° à N140° résultant d'une extension NNE-SSW, (2) la faille d'Aaraben dans sa partie NE est caractérisée par des zones de cisaillement ductiles normales, orientées N70° à N150° résultant d'une extension N-S et (3) l'âge de cet évènement extensif est compris entre 22 et 20 Ma. Les données paléomagnétiques disponibles, permettent de restaurer l'orientation initiale de cette extension, qui était approximativement E-O contemporaine de l'ouverture du bassin d'Alboran en position d'arrière-arc, au cours du Miocène inférieur. Au début de l'extension, les péridotites reposaient sur une croûte continentale partiellement fondue, et exhumées pendant cet évènement par la zone de cisaillement normale d'Aaraben. Le domaine d'Alboran a ensuite été affecté par plusieurs événements compressifs.

Mots clés : arc de Gibraltar / péridotites / filons granitiques / zones de cisaillement ductiles / datation ^{40}Ar–^{39}Ar / extension arrière arc

*Corresponding author: asmae.elbakili@geoazur.unice.fr

1 Introduction

The Gibraltar Arc is an arcuate orogenic system located in the extreme tip of the western Mediterranean Sea (Fig. 1). This orogen is composed of the Betics and the Rif mountain ranges, which consist mainly of stacked tectonic units thrust toward the Guadalquivir and the Gharb foreland Basins, in southern Spain and northern Morocco respectively (Fig. 1). The Betic-Rif Internal domain (Alboran Domain) includes the Ronda and Beni Bousera subcontinental peridotites, in the Spanish and Moroccan branches of the arc, respectively (Balanya and Garcia-Duenas, 1987).

This orogenic system is edified along the active margin of the western Mediterranean, as the final consequence of the Africa-Eurasia convergence accommodated since the Late Cretaceous by the subduction of the oceanic lithosphere (Dercourt *et al.*, 1986; Stampfli, 2000; Michard *et al.*, 2002; Verges and Fernandez, 2012; Platt *et al.*, 2013).

During the Early Neogene, the Alboran Basin formed in the core of this orogenic system. Nowadays, the delineation of the subducted slab under the Gibraltar Arc by seismic tomography offers considerable constraints on the western Mediterranean geodynamics. Henceforth, E-dipping subduction followed by slab rollback (Royden, 1993; Lonergan and White, 1997; Spakman and Wortel, 2004) is one of the processes accepted as a general consensus to explain the Alboran Basin opening (Gutscher and Malod, 2002; Spakman and Wortel, 2004; Jolivet *et al.*, 2006; Verges and Fernandez, 2012; Bezada *et al.*, 2013; Chertova *et al.*, 2014; Faccenna *et al.*, 2014; Van Hinsbergen *et al.*, 2014; Casciello *et al.*, 2015; Mancilla *et al.*, 2015; Villaseñor *et al.*, 2015; for review). The Betic-Rif Belt acquired subsequently its arcuate geometry and underwent tightening processes, resulting from important vertical-axis block rotations and compressive deformations related to Africa-Eurasia plate convergence (Platzman *et al.*, 1993; Saddiqi *et al.*, 1995; Platt *et al.*, 2003; Cifelli *et al.*, 2016; Crespo-Blanc *et al.*, 2016).

The Alboran Basin opening was accompanied by granitic dykes intrusion within the peridotites and the underlying and overlying crustal metamorphic units from the Internal Domain (Priem *et al.*, 1979; Zeck *et al.*, 1989; Rossetti *et al.*, 2010). Therefore, the understanding of the tectonic context at the time of the granitic dykes intrusion may reveal information on the timing and the mechanism of emplacement of the so-called subcontinental peridotites into the crust, a subject that remains a warm debate for decades (*e.g.*, Kornprobst, 1976; Sánchez-Rodríguez and Gebauer, 2000; Afiri *et al.*, 2011; Sanz de Galdeano and Ruiz Cruz, 2016; Bessière, 2019). However, the tectonic scenario related to these granitic dykes has to take into account the subsequent deformations that affected the Internal domain, such as block rotations related to the Gibraltar Arc tightening.

In the internal Rif (the southern part of the Alboran Domain), this event of granitic intrusion has been related to crustal thinning according to different tectonic scenarios (Chalouan *et al.*, 1995; Ouazzani-Touhami and Chalouan, 1995; Rossetti *et al.*, 2013; Romagny, 2014). In these contrasted proposed scenarios, the importance of the subsequent deformations following this magmatic event has not been studied.

The present work aims at constraining the polyphase deformation that affected the Alboran Basin and the Gibraltar Arc since the Early Neogene using structural and petrological analyses, and $^{40}Ar/^{39}Ar$ geochronology in the Beni Bousera area (Figs. 1 and 2). These new data are compared with data from equivalent geological systems in the northern branch of the Gibraltar Arc (Betics cordilleras), and new issues related to the peridotites emplacement mechanism and timing will be addressed.

2 Geological setting

The Rif belt is classically subdivided into three main domains (Fallot, 1937; Durand-Delga, 1972; Kornprobst, 1974; Chalouan *et al.*, 2008) (Fig. 1): (a) the External Domain, (b) the Flysch nappes, and (c) the Internal Domain (the Alboran Domain). The Internal Domain is common between the Betics and the Rif and comprises from top to bottom: the Dorsale Calcaire, the Ghomarides, and the Sebtides units (respectively Malaguides and Alpujarrides units in the Betics; Durand-Delga, 1972; Kornprobst, 1974; Chalouan *et al.*, 2008; Sanz de Galdeano, 2019). Under the Alpujarrides, the Nevado-Filabrides complex consists of nappe-stack of HP-LT metamorphic units only outcropping in the Central and Eastern Betics (*e.g.*, Platt *et al.*, 2013).

The Ghomarides units consist of low-grade to non-metamorphic Palaeozoic formations overlain by non-metamorphic Mesozoic-Cenozoic cover series. The Sebtides are subdivided into upper and lower Sebtides. The upper Sebtides are basically made up of Permian to Triassic series; part of these units exhibits mineral associations indicating high-pressure, low-temperature (HP-LT) conditions of metamorphism typical of subduction zones (Bouybaouène, 1993; Bouybaouène *et al.*, 1995). In the Beni Bousera massif, the lower Sebtides consist of crustal metamorphic units overlying ~2 km thick unit of peridotites and affected from bottom to top by high to low-grade HT-LP metamorphism (Milliard, 1959; Kornprobst, 1974; Bouybaouène *et al.*, 1998; El Maz and Guiraud, 2001; Gueydan *et al.*, 2015; Homonnay *et al.*, 2018) (Fig. 2). The lower Sebtides are thrust over the Monte Hacho orthogneisses in the Ceuta peninsula and Cabo Negro area (Kornprobst, 1974; Romagny, 2014; Homonnay *et al.*, 2018).

The Beni Bousera massif forms an open NW-SE antiform with the peridotites in the core overlain by the metapelites units (Fig. 2). The lowermost, granulitic metapelites (kinzigites) are associated to the peridotites within the Beni Bousera unit (Kornprobst, 1974). This unit is in turn overlain by the Filali unit, which includes migmatitic gneisses at its base followed upward by mica-schists. In the NE, the antiform is crosscuted by the NW-SE trending Aaraben fault, steeply dipping to the NE (Kornprobst, 1974; Reuber *et al.*, 1982; Chalouan *et al.*, 1995). This fault was interpreted as a reverse fault associated with the Beni Bousera major fold (Kornprobst, 1974), then as a normal fault (Chalouan *et al.*, 1995; Romagny, 2014).The Aaraben fault crosscuts in its northwestern branch the ESE-WNW Jenane En Nich normal fault dipping 40° to 60° toward the NE (Chalouan *et al.*, 1995). In the southeastern branch, the Aaraben fault is intercepted by the N-S Tararte-Taza fault.

Swarms of granitic dykes intrude the Beni Bousera unit (peridotites and kinzigites) and the migmatitic gneisses of the Filali unit (Kornprobst, 1974; Elbaghdadi *et al.*, 1996; Michard *et al.*, 2006; Rossetti *et al.*, 2010; Fig. 2). These intrusions induced local alteration of the ultramafic rocks (Hajjar *et al.*, 2017). Strong

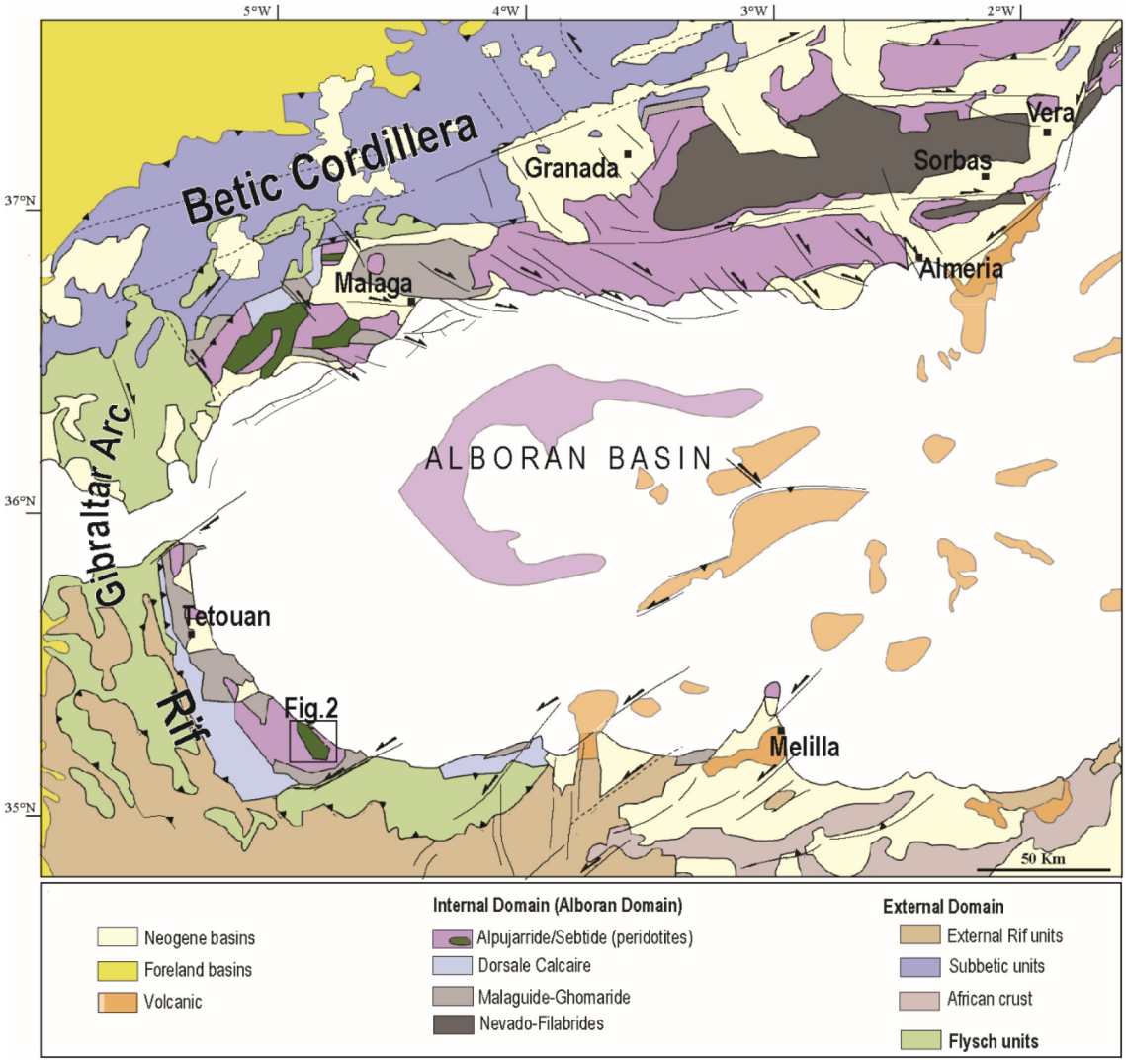

Fig. 1. Simplified structural map highlighting the position of the Alboran Domain and the localization of the current study (modified after Do Couto *et al.*, 2016).
Fig. 1. *Carte structurale simplifiée montrant la position du domaine d'Alboran et la localisation de la zone d'étude.*

serpentinization of the peridotites, followed by magnesite precipitation, is linked to fluid circulations that occur preferentially along the Aaraben fault (Hajjar *et al.*, 2015, 2016). The emplacement and the cooling of the granitic dykes are constrained at circa 22 Ma using ^{40}Ar–^{39}Ar on biotite and muscovite together with the U–Th–Pb method on zircon and monazite from the granite dykes (Rossetti *et al.*, 2013). The chemical signature of the dykes suggests a direct derivation from partial-melting of crustal protoliths, but with chemical compositions that differ from that of Beni Bousera and Filali units (Rossetti *et al.*, 2013). This testifies that the peridotites rest upon a different crustal unit. The granitic intrusions have been related to the Alboran Basin opening as a response to strike-slip tectonics associated with an E-W compression (Rossetti *et al.*, 2013), or alternatively to a radial extension event (Romagny, 2014).

3 Material and methods

3.1 Structural analyses

Structural data (faults with slickensides, ductile shear planes with the stretching lineation, fold axes, and cleavage planes) are collected from stations across three main cross-sections (two are orthogonal and one is parallel to the Beni Bousera antiform) (Fig. 2). A total amount of 77 faults and ductile shear zones, 19 cleavages and 4 folds axes were used in this work. The data were handled using the stereonet program (Allmendinger *et al.*, 2012; Cardozo and Allmendinger 2013, updated version 10.2.9, http://www.geo.cornell.edu/geology/faculty/RWA/programs/stereonet.html) in order to obtain their statistical distribution, using their strike and dip.

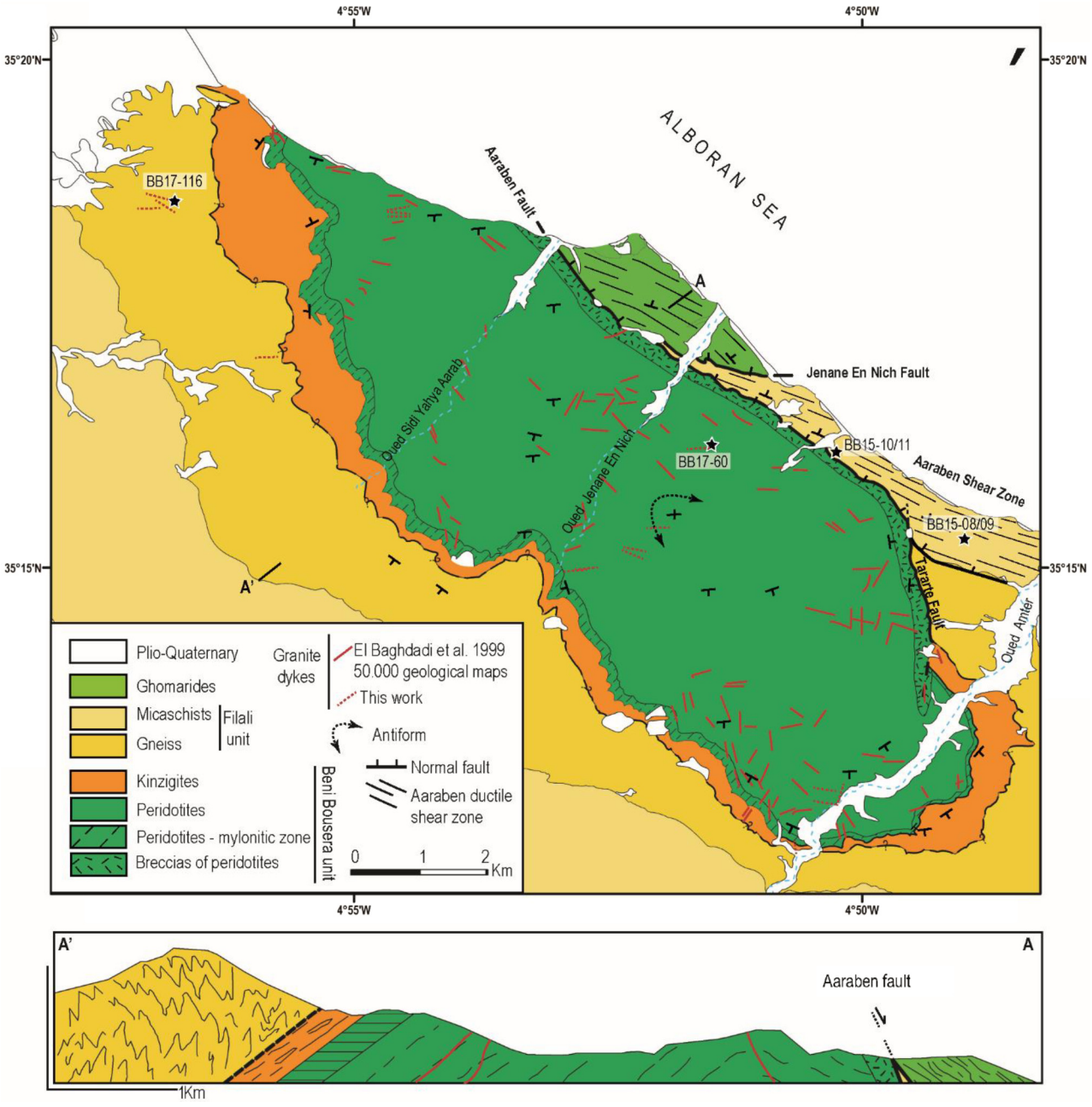

Fig. 2. Geological sketch map and cross-section of Beni Bousera area (modified after Kornprobst, 1959–1970; Kornprobst, 1966–1970; Reuber *et al.*, 1982; Elbaghdadi *et al.*, 1996). The stars represent samples location used for geochronology.
Fig. 2. *Carte et coupe géologique de la région de Beni Bousera.*

The determination of the principal stress axes (strike and plunge) and the stress ratio R ($R = \sigma2 - \sigma3/\sigma1 - \sigma3$) is performed using the right dihedron method (Angelier and Mechler, 1977; Delvaux and Sperner, 2003). The stress axes determination was carried out using scarce but efficient data providing all geometrical faults parameters and good kinematic observations, using (1) fault plane, slickenside and kinematics for faults and (2) shear planes, stretching lineation and kinematics for the ductile shear zones. We considered that brittle-ductile shear zones were suitable for palaeostress analyses by the right dihedron method because we are in conditions where the stretching lineations and the sense of movement can be measured directly on the shear plane and thus the movement vector can be resolved (Eisbacher, 1970; Srivastava *et al.*, 1995; Blewett and Czarnota, 2007).

The determination of the stress axes is carried out using the last version of the win_tensor program (version 5.8.9 updated 05/08/2019, http://damiendelvaux.be/Tensor/WinTensor/win-tensor.html).

The stress ratio allows the determination of the stress ellipsoid shape; radial extension ($\sigma1$ vertical, $0 < R < 0.25$), pure extension ($\sigma1$ vertical, $0.25 < R < 0.75$), transtension ($\sigma1$, vertical, $0.75 < R < 1$ or $\sigma2$ vertical, $0.75 < R < 1$), pure

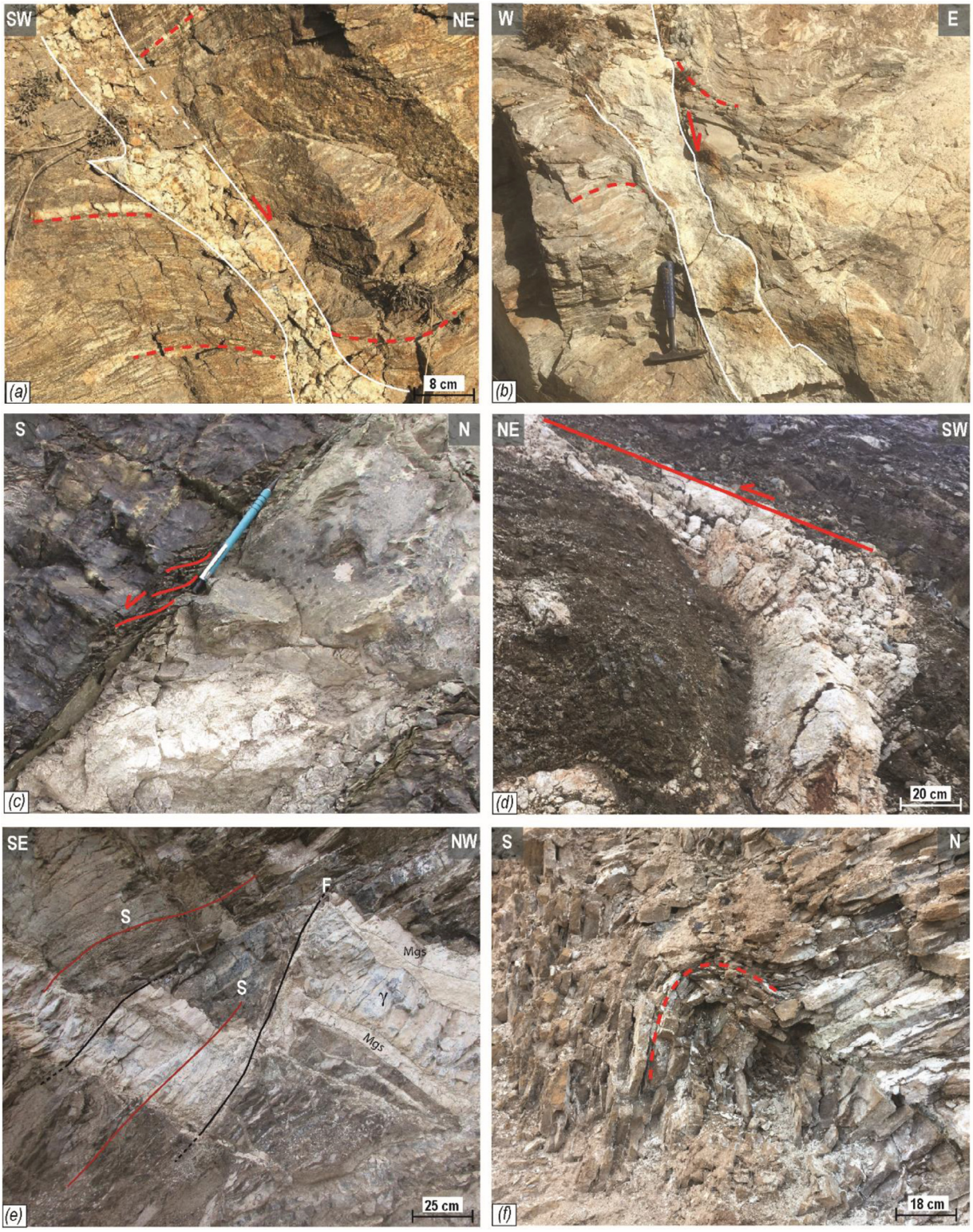

Fig. 3. Field view of granitic dykes and veins in regard to deformation. (a) NW-SE granitic vein crosscutting the migmatitic gneiss emplaced during normal shearing (N35°18'38", W04°56'48). (b) N-S granitic dyke crosscutting the Beni Bousera metamorphic unit, emplaced during normal shearing (N35°12'02", W04°50'29"). (c) E-W granitic dyke showing normal kinematic at the serpentinized peridotites wall (N35°18'29", W04°54'29"). (d) deformed granitic dyke by an inverse left-lateral strike-slip fault in the peridotites. (e) granitic dyke affected by normal left-lateral strike-slip fault and by spaced cleavage in the serpentinized peridotites (N35°12'40", W04°50'13"). (f) E-W fold affecting a spaced planar fabric in the serpentinized peridotites (N35°12'43", W04°50'07").

Fig. 3. *Photos de terrain montrant la relation entre les différents types de déformation dans le secteur de Beni Bousera.*

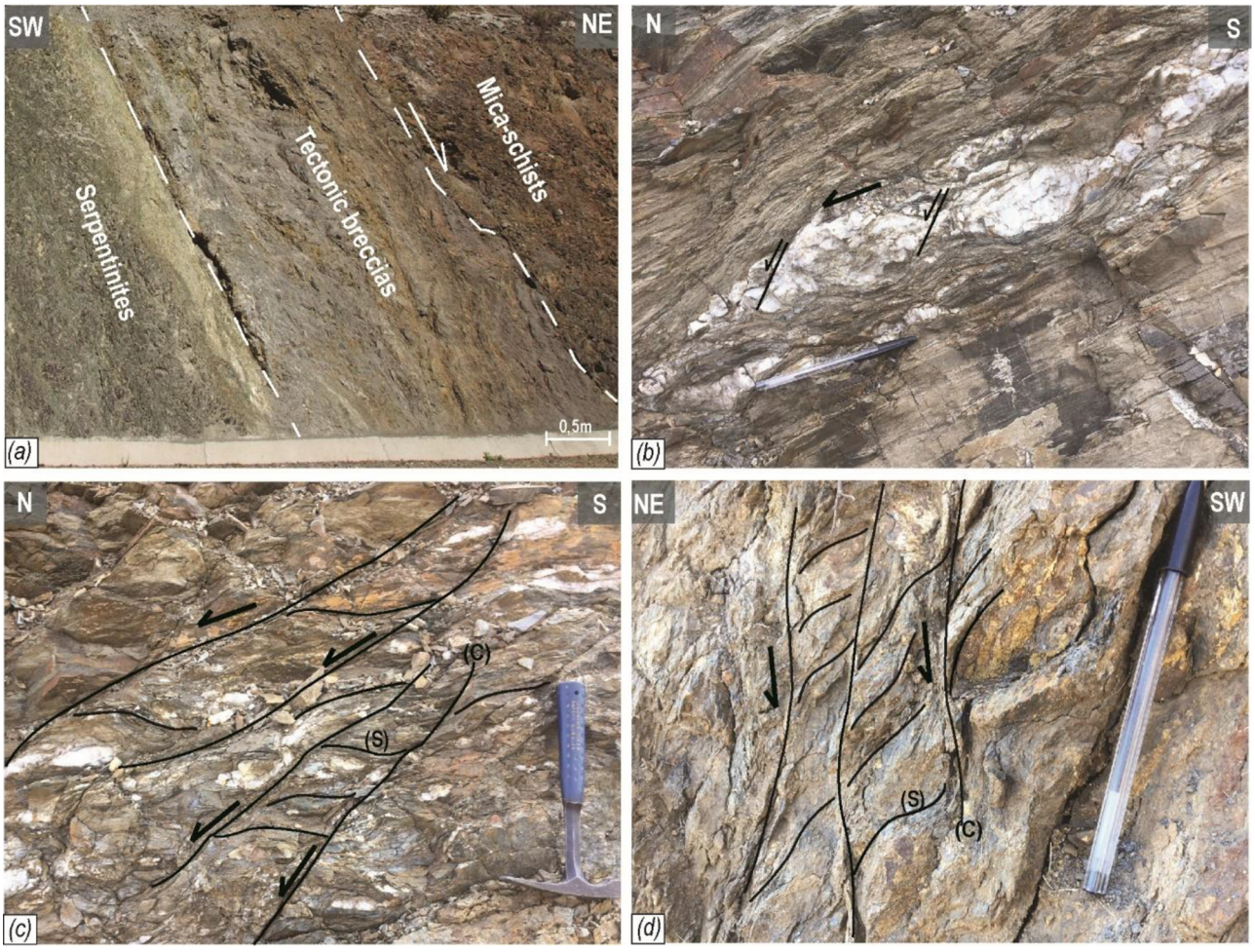

Fig. 4. Field photographs of the Aaraben area deformation. (a) the damaged zone of the Aaraben fault marked by a cataclasite corridor (N35°16'05", W04°50'23"). (b) Asymmetric boudinage of quartz-veinlet in a shear zone affecting the Filali mica-schists (N35°16'56", W04°51'25"). (c) extensional shear band in the mica-schists (N35°16'57", W04°51'25"). (d) S/C fabric in the serpentinized peridotite at the contact with the Filali unit (N35°16'52", W04°51'34").

Fig. 4. *Photographies de terrain de la déformation dans la région d'Aaraben.*

strike-slip ($\sigma 2$ vertical, $0.25 < R < 0.75$), transpression ($\sigma 2$ vertical, $0 < R < 0.25$ or $\sigma 3$ vertical, $0 < R < 0.25$), pure compression ($\sigma 3$, vertical, $0.25 < R < 0.75$) and radial compression ($\sigma 1$ vertical, $0.75 < R < 1$) (Delvaux, 1993).

3.2 ^{40}Ar–^{39}Ar analyses

Two samples of granitic dykes were collected; a sample from a dyke crosscutting the peridotites of the Beni Bousera unit (BB17-60) and a sample from a dyke crosscutting the gneiss of the Filali unit (BB17-116) (Fig. 2). Both biotite and muscovite grains were used for ^{40}Ar–^{39}Ar dating the sample BB17-116 and muscovite for the sample BB17-60. Four samples from the Aaraben normal ductile shear zones were collected along the coastal road within small shear zones in the micaschists of the Filali unit (BB15-08; BB15-09; BB15-10; BB15-11) (Fig. 2), from which only muscovite was used for ^{40}Ar–^{39}Ar dating. All analyzed muscovites sampled in the core of the shear zones are synkinematic (see Fig. 8).

Samples were crushed and sieved and the selected grain size for the crystals was in the order of 100–200 μm, then they were cleaned and dried. Muscovite and biotite were finally selected under a binocular microscope. Samples were packed in aluminum foil for irradiation in the core of the Triga Mark II nuclear reactor of Pavia (Italia) with several aliquots of the Taylor Creek sanidine standard (28.34 ± 0.08 Ma, Renne *et al.*, 1998) as flux monitor. Argon isotopic interferences on K and Ca were determined by irradiation of KF and CaF2 pure salts from which the following correction factors were obtained: ($^{40}Ar/^{39}Ar$) $K = 0.00969 \pm 0.00038$, ($^{38}Ar/^{39}Ar$) $K = 0.01297 \pm 0.00045$, ($^{39}Ar/^{37}Ar$) $Ca = 0.0007474 \pm 0.000021$ and ($^{36}Ar/^{37}Ar$) $Ca = 0.000288 \pm 0.000016$. Argon analyses were performed at Géosciences Montpellier Laboratory (France). The gas extraction and purification line consists of (a) an IR-CO2 laser of 100 kHz used at 3–15% power to heat samples during 60 s, (b) a lenses system for beam focusing, (c) a steel chamber, maintained at 10-8–10-9 bar, with a copper holder

in which 2 mm-diameter blind holes were milled, (d) two Zr–Al getters for purification of gases. Two different mass spectrometers were used: a MAP 215-50 noble gas mass spectrometer and a multi-collector mass spectrometer (Argus VI from Thermo–Fisher).

Aliquots of 40 to 50 grains of biotite and white micas were distributed as micropopulation five to ten grain deep in one and two holes of the copper holder, respectively, and were step heated. Blank analyses were performed every three sample analyses. Raw data of each step and blank were processed and ages were calculated using the ArArCALC-software (Koppers, 2002). The criteria for defining plateau ages are: (1) plateau steps should contain at least 70% of released ^{39}Ar, (2) there should be at least three successive steps in the plateau and (3) the integrated age of the plateau should agree with each apparent age of the plateau within a 2σ confidence interval. All the subsequent quote uncertainties are at the 2σ level including the error on the irradiation factor parameter J. With the MAP spectrometer the atmospheric contribution was difficult to determine precisely because of a high ^{36}Ar background on blanks. Thus, errors on individual ages are large (up to 5%) but we choose to present these results because they are complementary to those obtained on the Argus. Raw data can be downloaded from Supplementary Materials.

4 Results

4.1 Structural results

4.1.1 Granitic dykes

At the outcrop scale, granitic dykes and veins have diverse sizes with plurimetric length and centimetric to decimetric thickness (Figs. 3a–3e). They are mostly emplaced into major fractures, networks of faults and shear zones. Some of them are branched and may isolate blocks from the hosting rocks. A thin alteration envelope often occurs at the contact with the peridotites (Fig. 3). These alterations products consist mainly of magnesite, which offen occurs as veins (3 to 12 cm thick) filing fractures and fault zones, parallel to the granitic dykes (see the paragraph below).

Locally, in the metapelites, granitic dykes or veins were emplaced within normal ductile shear zones as evidenced by asymmetric bending of the foliation on both sides of the dykes (Figs. 3a and 3b). In the peridotites, dykes show evidence of deformation at the brittle-ductile transition, and at the dyke's walls, well-developed S/C planes are again indicative of normal shearing (*e.g.*, Fig. 3c). After their emplacement and cooling, the granitic dykes are affected by several deformation phases (Figs. 3d–3f) and they could have been significantly reoriented. Therefore, we performed analyses only of granitic dykes preserved from late deformation effects, at least at the local scale. Granitic dykes are globally E-W trending (Fig. 5a), with N70° to N140° distribution, and intermediate to steeply dip (40° to 80°). Few N-S and NNE-SSW dykes were observed at the scale of Beni Bousera massif and located mainly in the Oued Amter zone as previously mapped by Elbaghdadi *et al.* (1996) (Fig. 2) and studied by Rossetti *et al.* (2010, 2013). Fractures or faults in which magnesite veins are concentrated were also measured (Fig. 5a), they are trending parallel to granitic dykes with intermediate to steeply dip (35° to 90°). As this alteration product are concentrated in faults parallel to the granite dyke, and they provided the same kinematics, they are consequently considered as generated from the same deformation event. We determine the stress axes strike and plunge using structural elements obtained from these materials

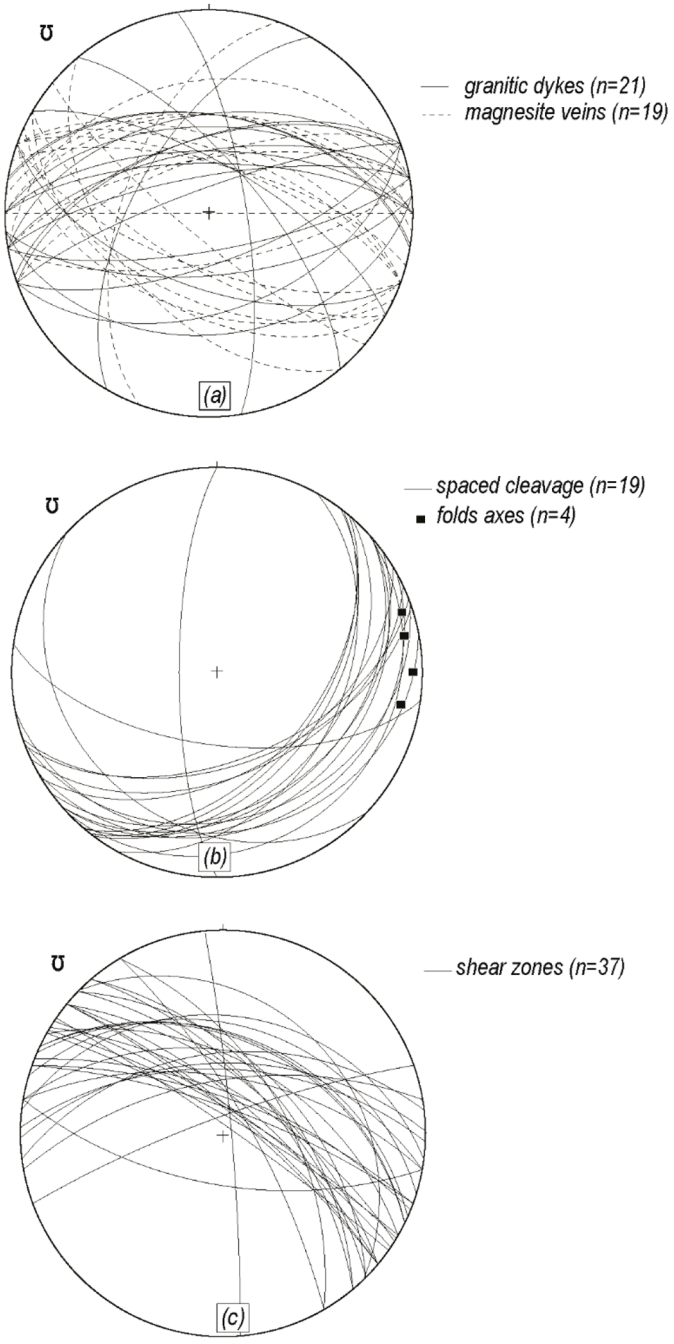

Fig. 5. Statistical distribution plot of structures in Beni Bousera massif. (a) granite dykes and magnesite veins. (b) spaced disjunctive cleavage and the folds axes. (c) shear zones in the NE of the Aaraben fault. Equal area projection, lower hemisphere.

Fig. 5. *Projection stéréographique des structures dans le massif de Beni Bousera. a) les filons granitiques et magnésites. b) clivage et axes des plis. c) zones de cisaillement dans la région d'Aaraben (projection de Schmidt, hémisphère inférieur).*

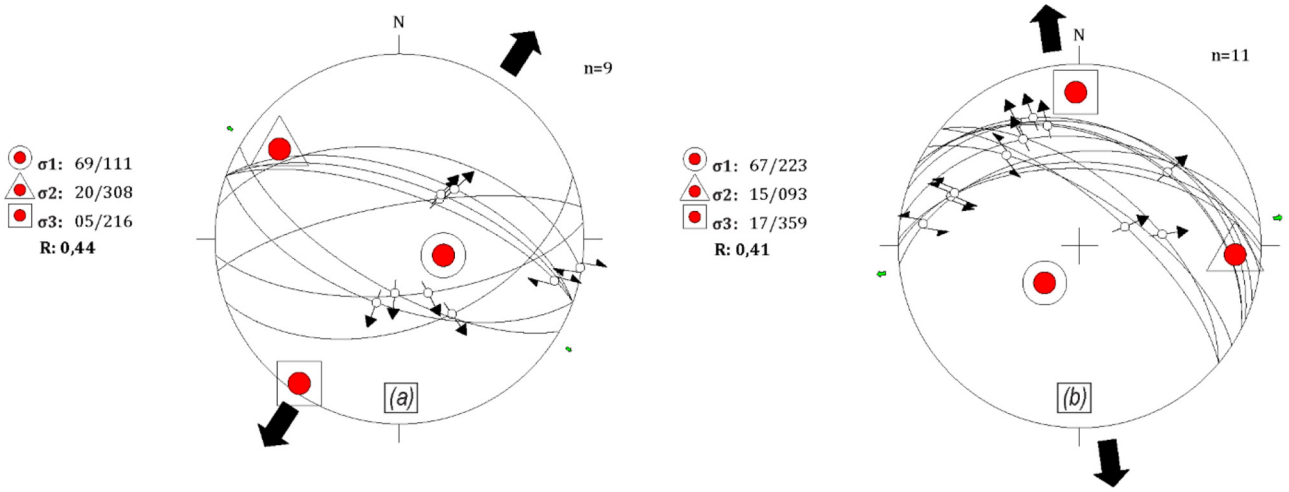

Fig. 6. Stress axes orientations, and the corresponding stress ratio R using the Right dihedron method. (a) faults related to granitic dykes and alteration. (b) shear zones in the NE of the Aaraben fault (Equal area projection-lower hemisphere).
Fig. 6. *Orientations des axes de contraintes et le rapport de contrainte R correspondant, en utilisant la méthode d'inversion du dièdre droit. a) failles associes aux filons granitiques et magnésites. b) zones de cisaillement dans la région d'Aaraben (projection de Schmidt, hémisphère inférieur).*

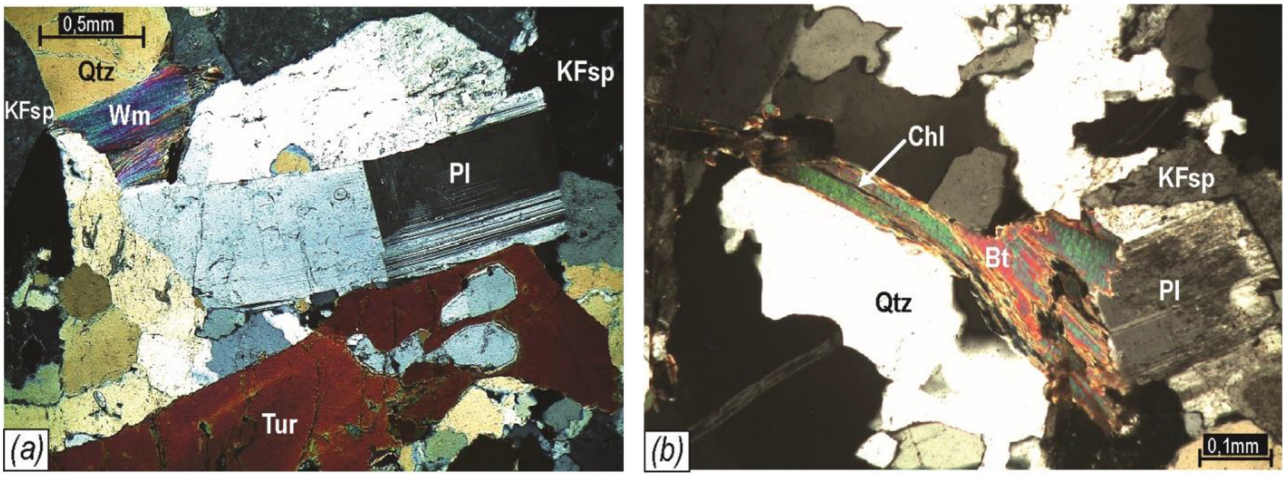

Fig. 7. Photomicrograph illustrating the mineralogy of the granitic dykes crosscutting Beni Bousera peridotites. (a) the main mineralogy of the granite, crossed polarized light; (b) chlorite after biotite, plane-polarized light. Mineral abbreviations after Kretz (1983).
Fig. 7. *Photomicrographies illustrant la minéralogie des filons granitiques intrusifs dans les péridotites de Beni Bousera.*

edge and/or from the host rock contact. Results give a N111°, 69° plunging maximum stress (σ1), a N308°, 20° plunging intermediate stress (σ2) and a N216°, 5° plunging minimum stress (σ3), with a stress ration R = 0.44 (σ1 vertical, 0.25 < R < 0.75), reflecting a pure extensional regime (Fig. 6a).

Concerning the late deformation events, the granitic dykes are affected by numerous late reverse and normal strike-slip faults (Figs. 3d and 3e; see Romagny, 2014). In the peridotite massif, a nearly NE-SW oriented penetrative spaced disjunctive cleavage (Powell, 1979; Passchier and Trouw, 2005) is observed in the granitic dykes and the peridotites (Figs. 3e and 5b). Afterward, this cleavage is affected by nearly E-W oriented folds (Figs. 3f and 5b).

4.1.2 Aaraben ductile shear zones

The Aaraben Fault was also the object of structural analyses (Fig. 2). The Aaraben fault is a N160°E northeastward dipping fault, marked by a few meters large cataclasites band developed under brittle conditions (Fig. 4a). The mirrors of the lensoid elements broadly parallel to the fault plane bear sub-vertical striae and displays kinematic indicators consistent with normal faulting.

In the north-east of the Aaraben fault (Fig. 2), numerous ductile shear zones, decimeter to a meter wide (Figs. 4b–d) crosscut the Ghomarides and the Sebtides units. All these shear zones constitute a deformation corridor of several hundred meters wide (Fig. 2).

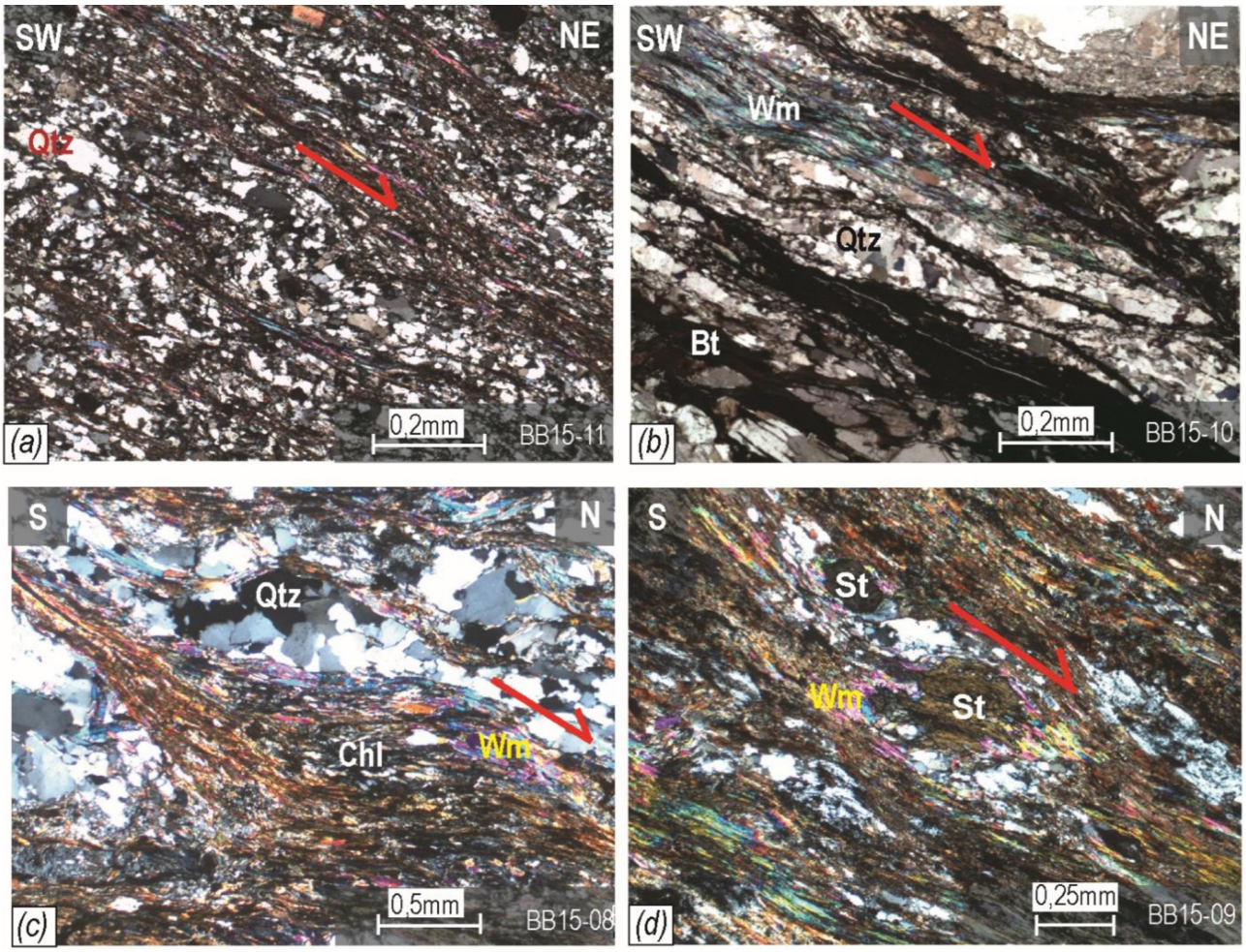

Fig. 8. Photomicrographs illustrating the microstructures and the associated recrystallizations in the Aaraben shear zone (crossed polarized light). (a) asymmetric intrafolial microfold with muscovite developed in the main foliation plane. (b) muscovite flakes and asymmetric quartz ribbons developed parallel to the foliation. (c) sigmoidal muscovite and chlorite within a shear zone (d) sigmoidal quartz ribbons and muscovite developed at the expense of staurolite porphyroclast. Mineral abbreviations after Kretz (1983).
Fig. 8. *Photomicrographies illustrant les relations entre cristallisation métamorphique et déformation dans la zone de cisaillement d'Aaraben.*

At the outcrop scale, the ductile shear zones are marked by the development of mylonitic foliation into centimeter to meter size deformation bands. The shear zones are also underlined by quartz veinlets (Fig. 4b) with aggregates of chlorite and white micas, reflecting pervasive fluid circulation during the development of the shear zone under greenschist facies conditions.

The ductile shear zones are globally trending NW-SE and moderately to steeply dipping toward the northeast (34° to 70°), (Fig. 5c). The stretching lineation is steeply dipping and shear-sense criteria such as asymmetric rotation of the foliation plane, asymmetric boudins, and S/C planes indicate a north-eastward collapse of the hanging wall, compatible with normal ductile shearing (Figs. 4b–4d).

The determination of the principal stress strike and plunge by the right dihedron gives a N223°, 67° plunging maximum stress ($\sigma1$) and N93°, 15°, plunging intermediate stress ($\sigma2$) and a N359°, 17° plunging minimum stress ($\sigma3$), with a stress ration $R = 0.41$ ($\sigma1$ vertical, $0.25 < R < 0.75$), reflecting pure extension (Fig. 6b).

4.2 Petrogrology

4.2.1 Granitic dykes petrography and chemistry

Petrographic analyses are performed at the thin section scale from granitic dykes crosscutting the peridotites and the migmatitic gneiss. All granitic dykes have a coarse-grained texture, two assemblages are observed; the first assemblage is composed of K-feldspar, quartz, plagioclase, white mica and tourmaline (Fig. 7a). Additionally, cordierite or biotite are also observed in some samples (*e.g.* Fig. 7b). The secondary assemblage consists of chlorite after biotite (Fig. 7b), pinite and sericite resulting from cordierite and feldspars alteration respectively. Accessory minerals are zircon and/or monazite and opaques minerals. According to Rossetti *et al.* (2013), these dykes are classified as biotite-cordierite bearing granodiorite to monzogranite or as tourmaline-muscovite bearing alkali-felspar granite.

4.2.2 Aaraben ductile shear zones

Petrographic investigations performed on the mica-schists from the shear zones allow to precise the mineralogical

assemblages associated with ductile deformation. Microstructures were observed from thin sections perpendicular to the foliation and parallel to the lineation to obtain kinematic constraints. The foliation plane is underlined by the planar disposition of muscovite and biotite as well as polycrystalline quartz ribbons (Figs. 8a and 8b). Biotite and staurolite porphyroclasts are destabilized and wrapped by muscovite and chlorite (Fig. 8d). Numerous shear criteria like microfolded quartz ribbons (Fig. 8a), S/C structures marked by deflections of quartz ribbons, chlorite and muscovites (Figs. 8b–8d) and recrystallized quartz grains in asymmetric pressure shadows around staurolite porphyroclasts (Fig. 8d) are typical of mylonitic rocks deformed by dominant simple shear and the kinematic indicators systematically provide a normal sense of shear.

4.3 ^{40}Ar–^{39}Ar dating

4.3.1 Granitic dykes

In the Beni Bousera area, muscovite and biotite from two samples of granitic dykes (BB17-60 and BB17-116) were analyzed:

- *Sample BB17-60*: a muscovite single grain yields a plateau age at 21.22 ± 0.42 Ma corresponding to 99% of ^{39}Ar released and to eight steps (Fig. 9). The inverse isochron for the plateau steps gives a concordant age at 21.18 ± 0.46 Ma (MSWD = 0.11; initial ^{40}Ar/^{36}Ar ratio of 298.6 ± 13.8) (see Supplementary Material 1). The plateau-age at 21.22 ± 0.42 Ma is considered as the best age estimate;
- *Sample BB17-116*: muscovite single grain (BB17-116M) yields a plateau age at 21.55 ± 0.13 Ma corresponding to 100% of ^{39}Ar released and to nine steps (Fig. 9). The inverse isochron for the plateau steps gives a concordant age at 21.41 ± 0.35 Ma (MSWD = 0.12; initial ^{40}Ar/^{36}Ar ratio of 298.7 ± 13.0) (see Supplementary Material 2). The plateau-age at 21.55 ± 0.13 Ma is considered as the best age estimate.

A biotite single grain (BB17-116B) yields a weighted age at 20.88 ± 0.21 Ma corresponding to 69% Ar released and to eight steps (Fig. 9). The staircase shape of the spectrum may suggest a reheating event younger than 20 Ma that may have slightly affected the plateau age. The inverse isochron for the plateau steps gives a concordant age at 21.31 ± 0.30 Ma (MSWD = 1.93; initial ^{40}Ar/^{36}Ar ratio of 280.0 ± 8.9) (see Supplementary Material 3). The plateau-age at 20.88 ± 0.21 Ma is considered as the best age estimate.

4.3.2 Aaraben ductile shear zones

White micas from samples into the shear zones in the Filali unit (BB15-08; BB15-09; BB15-10-BB15-11) were analyzed:

- *Sample BB15-08*: a white micas micropopulation yield a plateau age at 21.59 ± 0.06 Ma corresponding to 90% of ^{39}Ar released and to ten steps (Fig. 9). The inverse isochron for the plateau steps gives a concordant age at 21.59 ± 0.09 Ma (MSWD = 0.94; initial ^{40}Ar/^{36}Ar ratio of 296.1 ± 9.8) (see Supplementary Material 4). The plateau-age at 21.59 ± 0.06 Ma is considered as the best age estimate;
- *Sample BB15-09*: a white micas micropopulation yield a weighted age at 21.69 ± 0.15 Ma corresponding to 100% of ^{39}Ar released and to nine steps (Fig. 9). The inverse isochron for the plateau steps gives a concordant age at 21.67 ± 0.18 Ma (MSWD = 0.53; initial ^{40}Ar/^{36}Ar ratio of 303.6 ± 25.2) (see Supplementary Material 5). The plateau-age at 21.69 ± 0.15 Ma is considered as the best age estimate;
- *Sample BB15-10*: a white micas micropopulation yield a weighted age at 21.44 ± 0.12 Ma corresponding to 67% of ^{39}Ar released and to ten steps (Fig. 9). The inverse isochron for the plateau steps gives a concordant age at 21.43 ± 0.14 Ma (MSWD = 1.39; initial ^{40}Ar/^{36}Ar ratio of 298.2 ± 17.2) (see Supplementary Material 6). The plateau-age at 21.44 ± 0.12 Ma is considered as the best age estimate;
- *Sample BB15-11*: a white micas micropopulation yield a weighted age at 21.99 ± 0.21 Ma corresponding to 58% of ^{39}Ar released and to six steps (Fig. 9). The inverse isochron for the plateau steps gives a concordant age at 21.43 ± 0.14 Ma (MSWD = 1.54; initial ^{40}Ar/^{36}Ar ratio of 283.1 ± 52.9) (see Supplementary Material 7). The plateau-age at 21.99 ± 0.21 Ma is considered as the best age estimate.

5 Discussion

5.1 Structural evolution

Structural analyses underlined that granitic dykes are emplaced within major N70° to N140° faults, resulted from an NNE-SSW extension (N216°). This deformation is coeval (21–22 Ma) with the N70° to N150° ductile normal shear zones development which resulted from a nearly N-S extension (N179°). Thus, the stress axes orientation obtained from the shear zones and those obtained from faults related to the granitic dykes form an acute angle of 37° (Fig. 6). This variation could be explained either by different rheological response of the peridotites relative to the metapelites or either by a late effect of the Aaraben fault kinematics.

Indeed, as suggested by Romagny *et al.* (2014), faults acting under brittle conditions with similar direction as the Aaraben fault are responsible for the present-day uplift of the internal Rif. Moreover, Chalouan *et al.* (1995) described a vertical displacement of 4–5 km since the Neogene along the Aaraben fault. Our work highlights that most of this vertical movement was accommodated by a large NW-SE trending ductile normal shear zones system acting under greenschist facies metamorphic conditions. Such P/T environment implies an exhumation of the peridotites from at least the ductile-brittle transition. The paleomagnetic data available in the vicinity of the Beni Bousera massif indicate a 76° ± 13° (Saddiqi *et al.*, 1995), 72 ± 12° (Berndt *et al.*, 2015) counter-clockwise rotation since the Miocene. Hence the initial orientation of extension was comprised between NE-SW and ESE-WNW at 21 Ma. At that time, the restored subduction trench in front of the Alboran Domain was ~N-S (*e.g.* Spakman and Wortel, 2004; Verges and Fernandez, 2012). Hence the restored direction of extension was roughly normal to the restored subduction trench (Fig. 10a).

Regarding the tectonic context, our interpretation with an E-W extensional regime associated to a non-coaxial deformation contrasts with radial extension associated to the

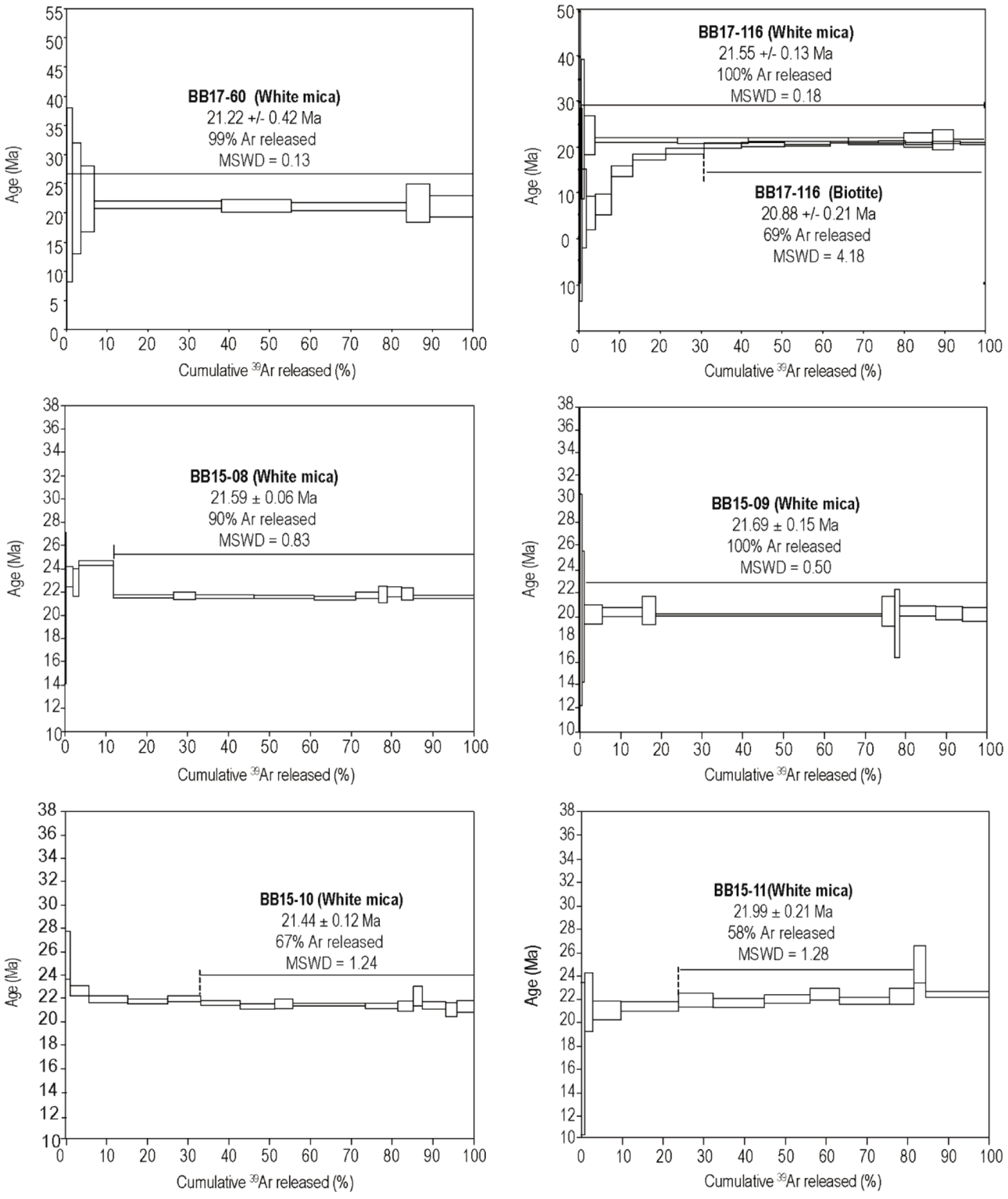

Fig. 9. $^{40}Ar/^{39}Ar$ age spectra as a function of ^{39}Ar released. The error boxes of each step are at the 2σ level. The error of the plateau ages (P) is given at the 2σ level. Ages were calculated using the Ar–Ar Calc software (Koppers, 2002). Raw data is presented in Supplementary Data.
Fig. 9. *Spectres d'âge $^{40}Ar/^{39}Ar$ en fonction du ^{39}Ar libéré.*

exhumation of the lower Sebtites units (Romagny, 2014) or strike-slip tectonic regime controlled by a roughly E-W oriented compression (Rossetti *et al.*, 2013), that were previously proposed for the Beni Bousera area.

The major extensional event that caused the exhumation of the peridotites and the emplacement of the granite dykes at 20–22 Ma was followed by late compressional events mainly evidenced by NE-SW cleavage and E-W folding.

5.2 Geochronological evolution

The muscovites from the two samples of granitic dykes crosscutting the peridotites of the Beni Bousera unit and the gneiss of the Filali unit yielded concordant ages at 21.22 ± 0.42 Ma and 21.55 ± 0.13 Ma respectively. The weighted average at 21.38 Ma is considered as the best age estimate. The biotite yielded an age at 20.88 ± 0.21 Ma which is slightly younger than the muscovites ages, which could be explained by a very rapid emplacement and cooling of the granitic dykes from 21.68 Ma to 20.67 Ma. The structural data highlight that the granitic dykes emplaced in normal faults, reflecting an extensional context (Fig. 3). On the other hand, within the normal ductile shear zones in the Filali unit, all the white micas yielded concordant ages, with a weighted average age at 21.68 Ma. Muscovites from the mica-schists sampled in the core of these shear zones are clearly synkinematic prophyroblasts that have grown or at least recrystallized during the development of the normal shear zones under greenschist facies metamorphic conditions (Fig. 8). Thus, as granitic dykes emplacement and normal ductile shear zones give the same age at circa 21 Ma, we consider that the ages around 21 Ma correspond to an extensional event.

These ages are similar to those obtained by previous authors in the internal Rif (Elbaghdadi *et al.*, 1996; Michard *et al.*, 2006; Rossetti *et al.*, 2010; Homonnay *et al.*, 2018) and also in the Betics where similar granitic dykes intruded the Ronda peridotites (Priem *et al.*, 1979; Zeck *et al.*, 1989; Cuevas *et al.*, 2006). (U-Th)/He and apatite fission track ages obtained on crustal rocks from the internal Rif are comprised between 17.8 and 14.1 Ma, suggesting that the exhumation in the Alboran Domain continues to develop after 21 Ma (Azdimousa, 1999; Azdimousa *et al.*, 2014; Romagny, 2014; Romagny *et al.*, 2014).

This extensional event occurred during the opening of the Late Oligocene to Early Miocene sedimentary basins of Fnideq and Sidi Abdeslam (Feinberg *et al.*, 1990; Ouazzani-Touhami and Chalouan, 1995; El Kadiri *et al.*, 2006; Serrano and Guerra-Merchán, 2007; Hlila *et al.*, 2008). Biostratigraphic analyses in these basins established the duration of sedimentation between the Late Oligocene and the Middle Burdigalian (Feinberg *et al.*, 1990; Hlila *et al.*, 2008). The deposits unconformably overlay the Ghomarides nappes contact, attesting that (i) nappes stacking was prior to Aquitanian and (ii) the metamorphic basement was exposed at the surface at that time (Michard *et al.*, 2006; Serrano *et al.*, 2006).

In the Internal Rif, the timing of the late compressional events is poorly constrained, due to the lack of precise sedimentary markers and geochronological data. The time range for these events is post Burdigalian (age for the youngest folded sediments in the Fnideq and Sidi Abdeslam Basins Hlila *et al.*, 2008) and prior to Early Zanclean (age of the oldest unfolded sediments in the Tirinesse Basin, Saji and Chalouan, 1995; Cornée *et al.*, 2014).

However thermal modeling using (U-Th)/He apatite data, $^{40}Ar/^{39}Ar$ and K/Ar data on biotite, zircon, and apatite fission track highlights that the rocks suffered a rapid to moderate cooling between 22.5 and 18 Ma, a re-heating between 18 and 15 Ma, then a rapid cooling and an exhumation to the surface at around 13 Ma (Azdimousa *et al.*, 2014; Romagny *et al.*, 2014). These authors interpreted the re-heating during the late Burdigalian-Early Langhian as a renewal in thrusting and burying of the internal units during a compressional event (back-thrusting).

6 Geodynamic implication

6.1 The Rif belt

The exhumation of the Beni Bousera peridotites mechanism and timing are strongly debated and different scenarios are proposed: (1) a pre-Alpine exhumation by crustal thinning followed by thrusting during the Alpine orogeny (Reuber *et al.*, 1982; Chalouan *et al.*, 2001; Chalouan and Michard, 2004) and (2) an Early Miocene exhumation due to an extensional regime in a back-arc context accommodated by low angle lithospheric shear zone located on top of the peridotites (Afiri *et al.*, 2011; Álvarez-Valero *et al.*, 2014; Frets *et al.*, 2014; Bessière, 2019). In the Ceuta Peninsula, Homonnay *et al.* (2018) demonstrated that the tectonic coupling between mantle peridotites and crustal metamorphic rocks occurred at a depth of 20–30 km under high-temperature conditions during crustal thickening at ~ 30 Ma. The peridotites were subsequently exhumed during the extensional event at ~ 21 Ma. Our data show that the peridotites were located somehow upon a partially melted continental crust during dyke's intrusion, and were exhumed by the Aaraben shear zone from at least the ductile-brittle transition at 21 Ma, which is in line with the second exhumation model cited above.

Following this extension event, major compressional events were recognized in the Beni Bousera area: a shortening phase associated to the NW-SE Beni Bousera antiform (Reuber *et al.*, 1982) and a nearly N-S shortening phase, evidenced by E-W folds (this work) and by NE/SW sinistral and NW/SE dextral conjugate strike-slip faults (Romagny, 2014).These compressional events were also described in the northern part of the Internal Rif (Chalouan, 1986; Vitale *et al.*, 2014, 2015; Homonnay *et al.*, 2018; Homonnay, 2019), where they folded the Fnideq Basin (Feinberg *et al.*, 1990) and are therefore post-Burdigalian. At the scale of the Internal Rif, the first compressional event produced regional-scale open folds like the Beni Mezala and Beni Bousera antiforms parallel to the belt. The timing of this compressional event is difficult to determine precisely due to the lack of biostratigraphic markers associated with sedimentary basins during this period. However, it could be related to the re-heating recorded by low-temperature thermochronometry between 18 and 15 Ma ascribed to back-thrusting and burying of the Internal Zones (Romagny *et al.*, 2014).

The second compressional phase caused nearly E-W trending open folds, posteriorly to the Burdigalian (Fnideq Basin, Hlila *et al.*, 2008) and prior to the Pliocene (Oued Laou and Tirinesse Basins, Cornée *et al.*, 2014).

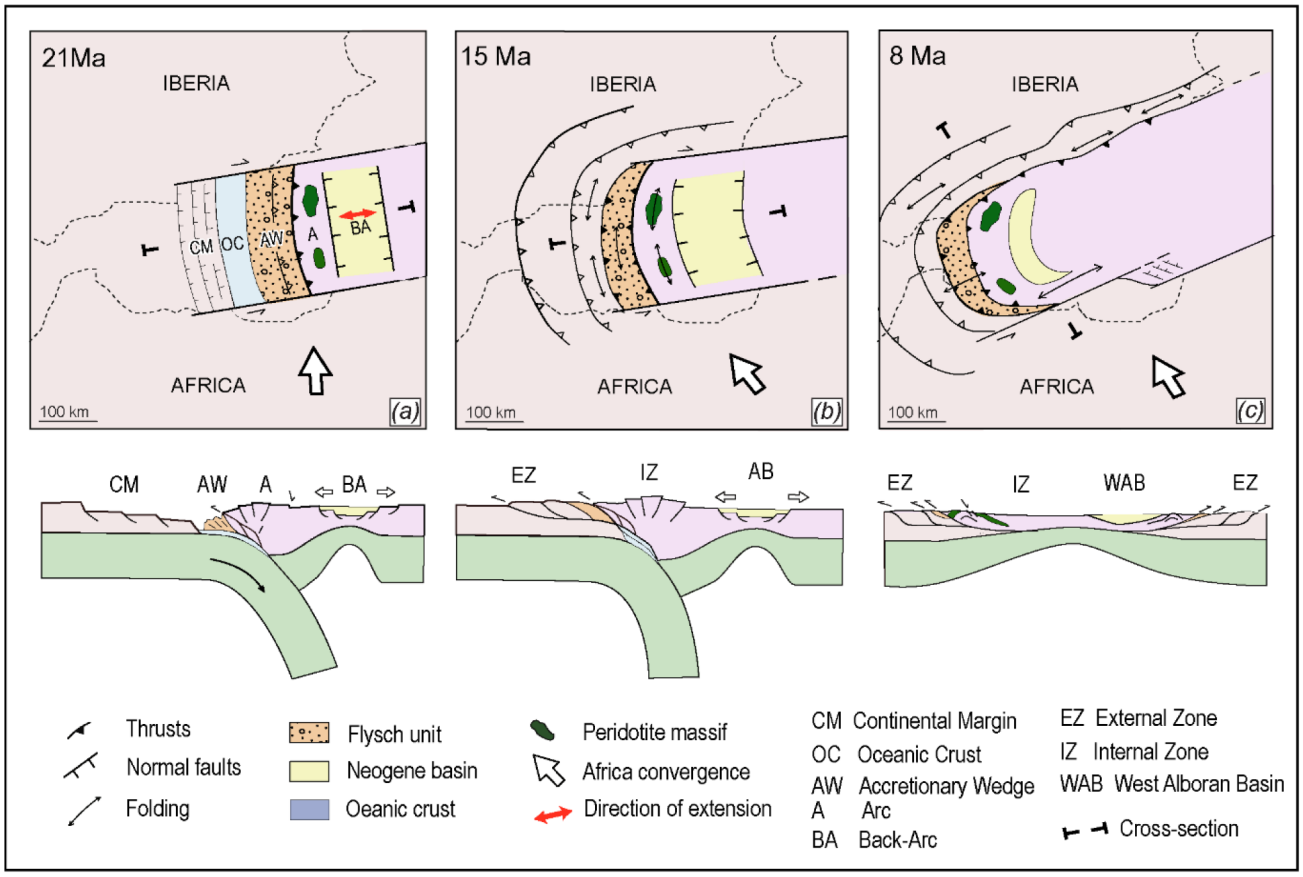

Fig. 10. Cartoons showing Miocene paleogeographic evolution of the Alboran Basin (map and cross-section) adapted from reconstructions by Do Couto *et al.* (2016), Crespo-Blanc *et al.* (2016) and Jolivet *et al.* (2019). The cross-sections (a) and (b) are E-W trending while the (c) cross-section is N-S trending.
Fig. 10. *Reconstitutions géodynamiques.*

6.2 Comparison with the Betic cordillera

In the Internal zone, the Nevado-Filabrides, the Alpujarrides and the Malaguides are separated by crustal-scale extensional shear zones (*e.g.*, García-Dueñas *et al.*, 1992; Jabaloy *et al.*, 1992; Lonergan and Platt, 1995;Augier *et al.*, 2005b; Platt *et al.*, 2013).

In Western Betics, the exhumation of the Alpujarride complex occurred during the Early Miocene (22 to 18 Ma) in a ≈ N-S to NNE-SSW (present coordinates) extensional setting (*i.e.*, Monié *et al.*, 1994; Crespo-Blanc, 1995; Platt *et al.*, 2006; Esteban *et al.*, 2013). The late exhumation of the Alpujarrides is also coeval with the development of Aquitano-Burdigalian extensional basins lying unconformably on the Malaguide and the Alpujarride complex (Serrano *et al.*, 2006, Serrano and Guerra-Merchán, 2007) and with the extensional development of the Alboran Basin (*e.g.*, Do Couto *et al.*, 2016). Paleomagnetic data and kinematic reconstructions suggest that the Western Betics were submitted to a ≈ 53° clockwise rotation since the Late Miocene (Lonergan *et al.*, 1993; Crespo-Blanc *et al.*, 2016). In this way, the Early Miocene extension was oriented ≈ WNW to NW-SE and, like in the Beni Bousera area, was orthogonal to the subduction trench.

In the Central and Eastern Betics, the Nevado-Filabride complex exhumation occurred during the Early to Late Miocene (*i.e.*, de Jong, 1991; Monié *et al.*, 1991; Platt *et al.*, 2005; Augier *et al.*, 2005a; Vazquez *et al.*, 2011) and was controlled by a ≈ E-W (present coordinates) regional-scale extension (Jabaloy *et al.*, 1992; Martínez-Martínez, 2006) evolving progressively to a NW-SE, then N-S (present coordinates) at the end of the Tortonian (Augier *et al.*, 2013). This extension also controlled the formation of extensional intra-mountain basins in the Eastern Betics, at the Nevado-Filabrides area (Augier *et al.*, 2013). Paleomagnetic data and kinematic reconstructions suggest that the Central Betics were submitted to a nearly 12° clockwise rotation since the upper Miocene (Crespo-Blanc *et al.*, 2016). This extension was then first oriented nearly ENE-WSW (parallel to the subduction trench) and progressively shifted to nearly NNW/SSE.

This E-W to ENE-WSW extension was widespread in the Gibraltar Arc during the Early-Middle Miocene and is considered as related to the westward migration of the Alboran Domain (Balanya *et al.*, 2012; Jolivet *et al.*, 2008). This strengthens the hypothesis proposing an important strain partitioning within the whole Gibraltar Arc during the Miocene

(Balanya *et al.*, 2012) with concomitant arc-perpendicular extension in the Western part of the Alboran Domain, arc-parallel extension in its Eastern part and arc-perpendicular compression within the orogenic wedge.

This simultaneous arc-perpendicular and arc-parallel extension in the Western and Eastern Betics respectively could reflect the particular crustal/mantle evolution of the eastern part of the Gibraltar Arc where the subduction is inactive since the Early Miocene and the slab tearing processes have probably occurred (Villaseñor *et al.*, 2015; Mancilla *et al.*, 2018).

Since the Tortonian, the entire Gibraltar Arc was submitted to a N-S to NNW-SSE compressional stress regime (Martínez-Martínez, 1997; Comas and Soto, 1999). This widespread compression has been recorded in the Eastern Betics (*e.g.*, Weijermars *et al.*, 1985; Galindo-Zaldívar *et al.*, 1993; Augier *et al.*, 2013; Do Couto, 2014), in the Western Betics (*e.g.*, Crespo-Blanc *et al.*, 2016), in the Alboran Domain (*e.g.*, Do Couto *et al.*, 2016). This compression event is also recognized offshore in the Alboran Basin where it results in WSW-ENE folding (Chalouan *et al.*, 1997, 2006; Mauffret *et al.*, 2007; Crespo-Blanc *et al.*, 2016; Do Couto *et al.*, 2016; Estrada *et al.*, 2017).

6.3 Consequences for the Gibraltar Arc and the Alboran Basin formation

The Early Miocene extension event is broadly described in the Rif and the Betics (García-Dueñas *et al.*, 1992; Galindo-Zaldívar *et al.*, 1993; Saji and Chalouan, 1995; Romagny, 2014). This event is contemporaneous with the opening of the Alboran back-arc Basin developed since the Oligocene in response to slab retreat towards the west (*e.g.*, Comas and Soto, 1999; Martínez-García *et al.*, 2011). In this context, crustal thinning (Fig. 10a), decompression and heat transfer from the hot asthenosphere mantle triggered partial melting of the crustal formations located under the peridotites and subsequent magmatic intrusion within the peridotites and the overlying crustal units (Rossetti *et al.*, 2013). Crustal thinning associated with ductile shear zones and normal faults was also responsible for the late exhumation of the Sebtides-Alpujarrides.

From the Late Early to the Middle Miocene the Gibraltar Arc was subjected to a period of shortening which resulted in the formation of an orogenic wedge with thrusting of the Internal zones upon the External zones toward the Rharb and the Guadalquivir Basins and back-thrusting in the internal zones toward the Alboran Basin (Chalouan *et al.*, 2008) (Fig. 10b). In this scenario, the arc-perpendicular shortening is the consequence of the collision between the Alboran Domain, assigned to the upper plate of the subduction complex, the Flysch nappes, and the External domain, corresponding to the accretionary prism and to lower plate paleomargin respectively (Fig. 10b).

During the Late Miocene, a N-S to NNW-SSE compressional event induced a tightening of the Gilbraltar Arc controlled by the Europe-Africa convergence that drastically altered its geometry (Crespo-Blanc *et al.*, 2016) (Fig. 10c).

7 Conclusion

The main outcomes of this study are as follows. In the Beni Bousera area, the granitic dykes were emplaced within nearly E-W normal faults at 21 Ma, and the NW-SE oriented Aaraben normal shear zones are also dated between 22 to 20 Ma. Granitic dykes and normal shear zones were generated in response to NNE-SSW extension (actual coordinate). Based on available paleomagnetic data, the tectonic setting which affected the Alboran Domain during the Early Miocene was a nearly E-W extension related to the opening of the back-arc Alboran Basin. At the time of the extension, the subcontinental peridotites were located upon a partially melted continental crust at least from the brittle-ductile transition. After this extension, two compressional events are evidenced successively by NW-SE and E-W folds in the framework of Africa-Eurasia convergence.

Supplementary Material

Supplementary Materials 1–7.
The Supplementary Material is available at http://www.bsgf.fr/10.1051/bsgf/2020008/olm.

Acknowledgment. The authors thank André Michard, Jesús Galindo Zaldívar, and the associate editor Romain Augier for their constructive reviews that improved the manuscript. This work has been funded by FP7-IRSES-MEDYNA project.

References

Afiri A, Gueydan F, Pitra P, Essaifi A, Précigout J. 2011. Oligo-Miocene exhumation of the Beni-Bousera peridotite through a lithosphere-scale extensional shear zone. *Geodinamica Acta* 24: 49–60. DOI: 10.3166/ga.24.49-60.

Allmendinger RW, Cardozo N, Fisher D. 2012. Structural geology algorithms: Vectors and tensors. Cambridge University Press.

Álvarez-Valero AM, Jagoutz O, Stanley J, Manthei C, Maz A, El Moukadiri A, *et al*. 2014. Crustal attenuation as a tracer for the emplacement of the Beni Bousera ultramafic massif (Betico-Rifean belt). *Bullettin of the Geological Society of America* 126: 1614–1624. DOI: 10.1130/B31040.1.

Angelier J, Mechler P. 1977. Sur une méthode graphique de recherche des contraintes principales également utilisable en tectonique et en séismologie : la méthode des dièdres droits. *Bull. Soc. géol. Fr.* XIX (1): 1309–1318.

Augier R, Agard P, Monié P, Jolivet L, Robin C, Booth-Rea G. 2005a. Exhumation, doming and slab retreat in the Betic Cordillera (SE Spain):Insitu $^{40}Ar/^{39}AR$ ages and P-T-d-t paths for the Nevado-Filabride complex. *J. Metamorph. Geol.* 23: 357–381. DOI: 10.1111/j.1525-1314.2005.00581.x.

Augier R, Jolivet L, Robin C. 2005b. Late Orogenic doming in the eastern Betic Cordilleras: Final exhumation of the Nevado-Filabride complex and its relation to basin genesis. *Tectonics* 24: 1–19. DOI: 10.1029/2004TC001687.

Augier R, Jolivet L, Do Couto D, Negro F. 2013. From ductile to brittle, late- to post-orogenic evolution of the Betic Cordillera: Structural insights from the northeastern internal zones. *Bulletin de*

la Société Géologique de France 184: 405–425. DOI: 10.2113/gssgfbull.184.4-5.405.

Azdimousa A. 1999. Géodynamique et exhumation des bordures méridionales de la mer d'Alboran entre le massif de Béni Bouzera et le Cap des Trois Fourches (Rif, Maroc). Apports de la méthode d'analyse par traces de fission. Thèse Doctorat d'État, Oujda (Maroc), 221 p.

Azdimousa A, Bourgois J, Poupeau G, Vázquez M, Asebriy L, Labrin E. 2014. Fission track thermochronology of the Beni Bousera peridotite massif (Internal Rif, Morocco) and the exhumation of ultramafic rocks in the Gibraltar Arc. *Arabian Journal of Geosciences* 7: 1993–2005. DOI: 10.1007/s12517-013-0924-3.

Balanya JC, Garcia-Duenas V. 1987. Les directions structurales dans le Domaine d'Alboran de part et d'autre du Détroit de Gibraltar. *Comptes Rendus de l'Académie des Sciences de Paris* Série II 304: 929–932.

Balanya JC, Crespo-Blanc A, Díaz-Azpiroz M, Expósito I, Torcal F, Perez-Pena V, *et al.* 2012. Arc-parallel vs back-arc extension in the Western Gibraltar arc: Is the Gibraltar forearc still active? *Geologica Acta* 10: 249–263.

Berndt T, Ruiz-Martínez VC, Chalouan A. 2015. New constraints on the evolution of the Gibraltar Arc from palaeomagnetic data of the Ceuta and Beni Bousera peridotites (Rif, northern Africa). *J. Geodyn.* 84: 19–39. DOI: 10.1016/j.jog.2014.09.014.

Bessière E. 2019. Évolution géodynamique des Zones Internes des Cordillères Bétiques (Andalousie, Espagne): Apports d'une étude pluridisciplinaire du Complexe Alpujárride Eloïse Bessière. Institut des Sciences de la Terre (To cite this version: HAL Id: tel-02392008).

Bezada MJ, Humphreys ED, Toomey DR, Harnafi M, Dávila JM, Gallart J. 2013. Evidence for slab rollback in westernmost Mediterranean from improved upper mantle imaging. *Earth Planetary Science Letters* 368: 51–60. DOI: 10.1016/j.epsl.2013.02.024.

Blewett RS, Czarnota K. 2007. Tectonostratigraphic architecture and uplift history of the Eastern Yilgarn Craton Module 3: Terrane Structure, Project Y1-P763. *Geoscience Australia Record* 2007 (15).

Bouybaouène ML. 1993. Étude pétrologique des métapelites des Sebtides superieures, Rif interne, Maroc: une évolution métamorphique de haute pression. Thèse Doctorat d'État, Université de Rabat, 160 p.

Bouybaouène ML, Goffé B, Michard A. 1995. High-pressure, low-temperature metamorphism in the Sebtides nappes, northern Rif, Morocco. *Geogaceta* 17.

Bouybaouène M, Michard A, Goffé B. 1998. High-pressure granulites on top of the Beni Bousera peridotites, Rif belt, Morocco: a record of an ancient thickened crust in the Alboran domain. *Bulletin de la Société Géologique de France* 2: 53–162.

Cardozo N, Allmendinger RW. 2013. Spherical projections with OSXStereonet. *Computers & Geosciences* 51: 193–205. DOI: 10.1016/j.cageo.2012.07.021.

Casciello E, Fernàndez M, Vergés J, Cesarano M, Torne M. 2015. The Alboran domain in the western Mediterranean evolution: the birth of a concept. *Bulletin de la Société Géologique de France* 186: 371–384. DOI: 10.2113/gssgfbull.186.4-5.371.

Chalouan A. 1986. Les nappes ghomarides (Rif septentrio- nal, Maroc). Un terrain varisque dans la chaîne alpine. Université de Strasbourg, 317 p.

Chalouan A, Michard A. 2004. The Alpine Rif Belt (Morocco): A Case of Mountain Building in a Subduction-Subduction-Transform Fault Triple Junction. *Pure and Applied Geophysics* 161: 489–519. DOI: 10.1007/s00024-003-2460-7.

Chalouan A, Ouazzani-Touhami A, Mouhir L, Saji R, Benmakhlouf M. 1995. Les failles normales à faible pendage du Rif interne (Maroc) et leur effet sur l'amincissement crustal du domaine d'Alboran. *Geogaceta* 17: 107–109.

Chalouan A, Saji R, Bally AW, Michard A. 1997. Neogene tectonic evolution of the southwestern Alboran Basin as inferred from seismic data off Morocco. *American Association of Petroleum Geologists* 81: 1161–1184.

Chalouan A, Michard A, Feinberg H, Montigny R, Saddiqi O. 2001. The Rif mountain building (Morocco): a new tectonic scenario. *Bulletin de la Société Géologique de France* 172: 603–616. DOI: 10.2113/172.5.603.

Chalouan A, Galindo-Zaldívar J, Akil M, *et al*. 2006. Tectonic wedge escape in the southwestern front of the Rif Cordillera (Morocco). *Geological Society of London*, Special Publication 262: 101–118. DOI: 10.1144/GSL.SP.2006.262.01.06.

Chalouan A, Michard A, El Kadiri K, *et al*. 2008. The Rif belt. In : Michard A, ed. *The Geology of Morocco*. Berlin: Springer, pp. 203–302. DOI: 10.1007/978-3-540-77076-3_5.

Chertova M, Spakman W, Geenen T, van den Breg A, van Hinsbergen DJJ. 2014. Underpinning tectonic reconstructions of the western Mediterranean region with dynamic slab evolution from 3D numerical modeling. *Journal of Geophysical Research Solid Earth* 119: 5876–5902. DOI: 10.1002/2014JB011150.

Cifelli F, Caricchi C, Mattéi M. 2016. Formation of arc-shaped orogenic belts in the Western and Central Mediterranean: a palaeomagnetic review. In : Pueyo EL, Cifelli F, Sussman AJ, Oliva-Urcia B, eds. *Palaeomagnetism in fold and thrust belts: New perspectives*. *Geological Society, London Special Publications* 425: 37–63.

Comas MC, Soto JI. 1999. Brittle deformation in the metamorphic basement at Site 976: implications for middle Miocene extensional tectonics in the Western Alboran Basin. *Proceedings of the Ocean Drilling Program Scientific Results* 161: 331–344. DOI: 10.2973/odp.proc.sr.161.226.1999.

Cornée JJ, Münch P, Melinte-Dobrinescu M, *et al*. 2014. The Early Pliocene reflooding in the Western Mediterranean: New insights from the rias of the Internal Rif, Morocco. *Comptes Rendus Géosciences* 346: 90–98. DOI: 10.1016/j.crte.2014.03.002.

Crespo-Blanc A. 1995. Interference pattern of extensional fault systems: a case study of the Miocene rifting of the Alboran basement (North of Sierra Nevada, Betic Chain). *Journal of Structural Geology* 17: 1559–1569. DOI: 10.1016/0191-8141(95)E0044-D.

Crespo-Blanc A, Comas M, Balanyá JC. 2016. Clues for a Tortonian reconstruction of the Gibraltar Arc: Structural pattern, deformation diachronism and block rotations. *Tectonophysics* 683: 308–324. DOI: 10.1016/j.tecto.2016.05.045.

Cuevas J, Esteban JJ, Tubia JM. 2006. Tectonic implications of the granite dyke swarm in the Ronda peridotites (Betic Cordilleras, Southern Spain). *Journal of the Geological Society of London* 163: 631–640. DOI: 10.1144/0016-764905-038.

Delvaux D. 1993. The Tensor program for paleostress reconstruction: examples from the east African and the Baikal rift zones. *Terra Nova* 5: 216.

Delvaux D, Sperner B. 2003. New aspects of tectonic stress inversion with reference to the TENSOR program. *Geological Society, London* Special Publications 212: 75–100. DOI: 10.1144/GSL.SP.2003.212.01.06.

de Jong K. 1991. Tectono-metamorphic studies and radiometric dating in the Betic Cordilleras (SE Spain) with implications for the dynamics of extension and compression in the Western Mediterranean area. PhD Thesis, Vrije Universiteit, Amsterdam, 204 p.

Dercourt J, Zonenshain LP, Ricou LE, *et al*. 1986. Geological evolution of the Tethys belt from the Atlantic to the Pamirs since the Lias. *Tectonophysics* 123: 241–315.

Do Couto D. 2014. Evolution géodynamique de la Mer d'Alboran par l'étude des bassins sédimentaires. PhD Thesis, University Pierre et Marie Curie, 552 p.

Do Couto D, Gorini C, Jolivet L, *et al*. 2016. Tectonic and stratigraphic evolution of the Western Alboran Sea Basin in the last 25Myrs. *Tectonophysics* 677–678: 280–311. DOI: 10.1016/j.tecto.2016.03.020.

Durand-Delga M. 1972. La courbure de Gibraltar, extrémité occidentale des chaines alpines, unit l'Europe et L'Afrique. *Eclogae Geologicae Helvetia* 65: 267–278. DOI: 10.5169/seals-164091.

Eisbacher GH. 1970. Deformation mechanics of mylonitic rocks and fractured granites in Cobequid Mountains, Nova Scotia. *Canada Geological Society of America Bulletin* 81: 2009–2020.

El Kadiri K, Chalouan A, Bahmad A, Salhi F, Liemlahi H. 2006. "Transgressive washing" concept: a sequence stratigraphic approach for calci- and siliciclastic turbidites. Tectonics of the Western Mediterranean and North Africa. *Geological Society of London* Special Publications 262: 45–54. DOI: 10.1144/GSL.SP.2006.262.01.02.

El Maz A, Guiraud M. 2001. Paragenèse à faible variance dans les métapelites de la serie de Filali (Rif interne marocain) : description, interprétation et conséquences géodynamique. *Bulletin de la Société Géologique de France* 172: 469–485.

Elbaghdadi M, Tabit A, Kornprobst J, Duthou JL. 1996. Les injections acides dans le massif des Beni Bousera et son enveloppe métamorphique : conséquence sur l'évolution du métamorphisme et la cinématique. *Notes et Mémoires du Service géologique du Maroc* 387: 33–44.

Esteban JJ, Tubía JM, Cuevas J, *et al*. 2013. Insights into extensional events in the Betic Cordilleras, southern Spain: New fission-track and U-Pb SHRIMP analyses. *Tectonophysics* 603: 179–188. DOI: 10.1016/j.tecto.2013.05.027.

Estrada F, Galindo-Zaldívar J, Vázquez JT, Ercilla G, D'Acremont E, Alonso B, *et al.* 2017. Tectonic indentation in the central Alboran Sea (westernmost Mediterranean). *Terra Nova* 30: 24–33. DOI: 10.1111/ter.12304.

Faccenna C, Becker TW, Auer L, *et al*. 2014. Mantle dynamics in the Mediterranean. *Reviews of Geophysics* 52: 283–332. DOI: 10.1002/2013RG000444.

Fallot P. 1937. Essai sur la géologie du Rif septentrional. *Notes mémoires du Service géologique du Maroc* 40: 553.

Feinberg H, Maaté A, Bouhdadi S, Durand-Delga M, Maaté M, Magné J *et al*. 1990. Signification des dépôts de l'Oligocène supérieur-Miocène inférieur du Rif interne (Maroc), dans l'évolution géodynamique de l'Arc de Gibraltar. *Comptes Rendus de l'Académie des Sciences de Paris* 310(II): 1487–1495.

Frets EC, Tommasi A, Garrido C. 2014. The Beni Bousera peridotite (Rif belt, Morocco): An oblique-slip low-angle shear zone thinning the subcontinental mantle lithosphere. *Journal of Petrology* 55: 283–313. DOI: 10.1093/petrology/egt067.

Galindo-Zaldívar J, González-Lodeiro F, Jabaloy A. 1993. Stress and palaeostress in the Betic-Rif cordilleras (Miocene to the present). *Tectonophysics* 227: 105–126. DOI: 10.1016/0040-1951(93)90090-7.

García-Dueñas V, Balanyá JC, Martínez-Martínez JM. 1992. Miocene extensional detachments in the outcropping basement of the northern Alboran Basin (Betics) and their tectonic implications. *Geo-Marine Lettes* 12: 88–95. DOI: 10.1007/BF02084917.

Gueydan F, Pitra P, Afiri A, Poujol M, Essaifi A, Paquette JL. 2015. Oligo-Miocene thinning of the Beni Bousera peridotites and their Variscan crustal host rocks, Internal Rif, Morocco. *Tectonics* 34: 1244–1268. DOI: 10.1002/2014TC003769.

Gutscher MA, Malod J, Rehault JP, *et al*. 2002. Evidence for active subduction beneath Gibraltar. *Geology* 30: 1071–1074. DOI: 10.1130/0091-7613(2002)030<1071:EFASBG>2.0.CO;2.

Hajjar Z, Wafik A, Constantin M. 2015. Magnesite Veins from Ultramafic Massif of Beni Bousera (Internal Rif, Morocco). *Tethys* 3: 152–162.

Hajjar Z, Wafik A, Constantin M, Bhilisse M. 2016. Process of serpentinization in the ultramafic massif of Beni Bousera (internal Rif, Morocco). *Arabian Journal of Geoscience* 9: 1–9. DOI: 10.1007/s12517-016-2507-6.

Hajjar Z, Gervilla F, Essaifi A, Wafik A. 2017. Mineralogical and geochemical features of the alteration processes of magmatic ores in the Beni Bousera ultramafic massif (north Morocco). *Journal of African Earth Sciences* 132: 47–63. DOI: 10.1016/j.jafrearsci.2017.04.022.

Hlila R, Chalouan A, El Kadiri K, *et al.* 2008. New stratigraphic data of the Oligo-Miocene transgressive cover of the Ghomaride units (Northern Internal Rif, Morocco): Implications on tectonosedimentary evolution. *Revista de la Sociedad Geológica de España* 21: 59–71. http://digital.csic.es/handle/10261/29426.

Homonnay E. 2019. Evolution tectono-métamorphique et chronologie de mise en place des unités métamorphiques du Rif interne (Maroc). PhD Thesis, Université Côte d'Azur, 300 p.

Homonnay E, Corsini M, Lardeaux JM, *et al*. 2018. Miocene crustal extension following thrust tectonic in the Lower Sebtides units (internal Rif, Ceuta Peninsula, Spain): Implication for the geodynamic evolution of the Alboran domain. *Tectonophysics* 722: 507–535. DOI: 10.1016/j.tecto.2017.11.028.

Jabaloy A, Galindo-Zaldívar J, González-Lodeiro F. 1992. The Mecina Extensional System: Its relation with the post-Aquitanian piggy-back Basins and the paleostresses evolution (Betic Cordilleras, Spain). *Geo-Marine Letters* 12: 96–103. DOI: 10.1007/BF02084918.

Jolivet L, Augier R, Robin C, Suc JP, Rouchy JM. 2006. Lithospheric-scale geodynamic context of the Messinian salinity crisis. *Sedimentary Geology* 188–189: 9–33.

Jolivet L, Augier R, Faccenna C, Negro F, Rimmele G, Agard P, *et al.* 2008. Subduction, convergence and the mode of backarc extension in the Mediterranean region. *Bulletin de la Societe Geologique de France* 179: 525–550. DOI: 10.2113/gssgfbull.179.6.525.

Jolivet L, Romagny A, Menant A. 2019. Géodynamique de la Méditerranée. *Géochronique* 149: 14–19. DOI: 10.1016/j.sedgeo.2006.02.004.

Koppers AAP. 2002. ArArCALCF software for $Ar/^{39}Ar$ age calculations. *Computer Geosciences* 28: 605–619.

Kornprobst J. 1959–1970. Carte géologique du Rif, région de Bou Ahmed, 1:50 000. Rabat: Service de la carte géologique.

Kornprobst J. 1966–1970. Carte géologique du Rif, région de Bab Berret, 1:50 000. *Notes serv. géol.* Maroc.

Kornprobst J. 1974. Contribution à l'étude pétrographique et structurale de la zone interne du Rif (Maroc septentrional). *Comptes Rendus de l'Académie des Sciences de Paris* 2: 21–40.

Kornprobst J. 1976. Signification structurale des péridotites dans l'orogenèse bético-rifain: arguments tirés de l'étude des détritus observés dans les sédiments paléozoïques. *Bull. Soc. géol. France* XVIII(3): 607–618.

Kretz R. 1983. Symbols for rock-forming minerals. *American Mineralogist* 68: 277–279.

Lonergan L, Platt JP. 1995. The Malaguide-Alpujarride boundary: a major extensional contact in the Internal Zone of the eastern Betic Cordillera, SE Spain. *J. Struct. Geol.* 17. DOI: 10.1016/0191-8141(95)00070-T.

Lonergan L, White N. 1997. Origin of the Betic-Rif mountain belt. *Tectonics* 16: 504–522. DOI: 10.1029/96TC03937.

Mancilla F, Booth-Rea G, Stich D. 2015. Slab rupture and delamination under the Betics and Rif constrained from receiver functions. *Tectonophysics* 663: 225–237. DOI: 10.1016/j.tecto.2015.06.028.

Mancilla F, Heit B, Morales J, Yuan X, *et al*. 2018. A STEP fault in Central Betics, associated with lateral lithospheric tearing at the northern edge of the Gibraltar arc subduction system. *Earth and Planetary Science Letters* 486: 32–40.

Martínez-García P, Soto JI, Comas M. 2011. Recent structures in the Alboran Ridge and Yusuf fault zonesbased on swath bathymetry and sub-bottom profiling: Evidence of active tectonics. *Geo-Marine Letters* 31: 19–36. DOI: 10.1007/s00367-010-0212-0.

Martínez-Martínez JMA. 1997. Mode of extensional tectonics in the southeastern Betics (SE Spain): Implications for the tectonic evolution of the peri-Alboran orogenic system. *Tectonics* 16: 205–225. DOI: 10.1029/97TC00157.

Martínez-Martínez JMA. 2006. Lateral interaction between metamorphic core complexes and less-extended, tilt-block domains: the Alpujarras strike-slip transfer fault zone (Betics, SE Spain). *Journal of Structural Geology* 28: 602–620.

Mauffret A, Ammar A, Gorini C, Jabour H. 2007. The Alboran Sea (Western Mediterranean) revisited with a view from the Moroccan Margin. *Terra Nova* 19: 195–203. DOI: 10.1111/j.1365-3121.2007.00734.x.

Michard A, Chalouan A, Feinberg H, Goffe B, Montigny R. 2002. How does the Alpine belt end between Spain and Morocco? *Bulletin de la Société Géologique de France* 173: 3–15. DOI: 10.2113/173.1.3.

Michard A, Negro F, Saddiqi O, Bouybaouène M, *et al*. 2006. Pressure- temperature-time constraints on the Maghrebide mountain building: Evidence from the Rif-Betic transect (Morocco, Spain), Algerian correlations, and geodynamic implications. *Comptes Rendus Geosciences* 338: 92–114. DOI: 10.1016/j.crte.2005.11.011.

Milliard Y. 1959. Les massifs métamorphiques et ultrabasiques de la zone paléozoïque interne du Rif. *Notes mémoires du Service géologique du Maroc* 18: 125–160.

Monié P, Galindo-Zaldivar J, Gonzales-Lodeiro F, Goffe B, Jabaloy A. 1991. $^{40}Ar/^{39}Ar$ geochronology of Alpine tectonism in the Betic Cordilleras (southern Spain). *Journal of the Geological Society of London* 148: 289–297.

Monié P, Torres-Roldán RL, García-Casco A. 1994. Cooling and exhumation of the Western Betic Cordilleras, $^{40}Ar/^{39}Ar$ thermochronological constraints on a collapsed terrane. *Tectonophysics* 238: 353–379. DOI: 10.1016/0040-1951(94)90064-7.

Ouazzani-Touhami M, Chalouan A. 1995. La distension de l'Oligocène supérieur à Burdigalien dans les nappes Ghomarides (Rif interne septentrional, Maroc). *Geogaceta* 17: 113–116.

Passchier CW, Trouw RAJ. 2005. Microtectonics. NewYork: Springer-Verlag, 366 p.

Platt JP, Allerton S, Kirker A, Mandeville C, Mayfield A, Platzman ES, Rimi A. 2003. The ultimate arc: Differential displacement, oroclinal bending, and vertical axis rotation in the External Betic-Rif arc. *Tectonics* 22. DOI: 10.1029/2001TC001321.

Platt J, Kelley SP, Carter A, Orozco M. 2005. Timing of tectonic events in the Alpujarride Complex, Betic Cordillera, southern Spain. *Journal of the Geological Society of London* 162: 451–462. DOI: 10.1144/0016-764903-039.

Platt JP, Soto JI, Kelley SP. 2006. Early Miocene continental subduction and rapid exhumation in the western Mediterranean. *Geology* 34: 981–984. DOI: 10.1130/G22801A.1.

Platt JP, Behr WM, Johanesen K, Williams JR. 2013. The Betic-Rif Arc and Its Orogenic Hinterland: a review. *Annual Review of Earth and Planetary Sciences* 41: 313–357. httpsoi.org/10.1146/annurev-earth-050212-123951.

Platzman ES, Platt JP, Olivier P. 1993. Palaeomagnetic rotations and fault kinematics in the Rif Arc of Morocco. *Journal of the Geological Society* 150: 707–718. DOI: 10.1144/gsjgs.150.4.0707.

Powell CM. 1979. A morphological classification of rock cleavage. *Tectonophysics* 58: 21–34. DOI: 10.1016/0040-1951(79)90320-2.

Priem HNA, Boelrijk NAIM, Hebeda EH, Oen IS, Verdurmen EAT, Verschure RH. 1979. Isotopic dating of the emplacement of the ultramafic masses in the Serrania de Ronda, Southern Spain. *Contribution to Mineraogy and Petrology* 70: 103–109. DOI: 10.1007/BF00371876.

Renne PR, Swisher CC, Deino AL, Karner DB, Owens TL, DePaolo DJ. 1998. Intercalibration of standards, absolute ages and uncertainties in $^{40}Ar/^{39}Ar$ dating. *Chemichal Geology* 145: 117–152. DOI: 10.1016/S0009-2541(97)00159-9.

Reuber I, Michard A, Chalouan A, Juteau T, Jermoumi B, 1982. Structure and emplacement of the Alpine- type peridotites from Beni Bousera, Rif, Morocco: A polyphase tectonic interpretation. *Tectonophysics* 82: 231–251. DOI: 10.1016/0040-1951(82)90047-6.

Romagny A. 2014. Évolution des mouvements verticaux néogènes de la chaîne du rif (nord-maroc) : apports d'une analyse structurale et thermochronologique. PhD Thesis, Nice-Sophia Antipolis University, 275 p.

Romagny A, Münch P, Cornée JJ, *et al*. 2014. Late Miocene to present-day exhumation and uplift of the Internal Zone of the Rif chain: Insights from low temperature thermochronometry and basin analysis. *Journal of Geodynamics* 77: 39–55. DOI: 10.1016/j.jog.2014.01.006.

Rossetti F, Theye T, Lucci F, *et al*. 2010. Timing and modes of granite magmatism in the core of the Alboran Domain, Rif chain, northern Morocco: Implications for the Alpine evolution of the western Mediterranean. *Tectonics* 29. DOI: 10.1029/2009TC002487.

Rossetti F, Dini A, Lucci F, Bouybaouenne M, Faccenna C. 2013. Early Miocene strike-slip tectonics and granite emplacement in the Alboran Domain (Rif Chain, Morocco): Significance for the geodynamic evolution of Western Mediterranean. *Tectonophysics* 608: 774–791. DOI: 10.1016/j.tecto.2013.08.002.

Royden LH. 1993. Evolution or retreating subduction boundaries formed during continental collision. *Tectonics* 12: 629–638.

Saddiqi O, Feinberg H, Elazzab D, Michard A. 1995. Paleomagnetism of the Beni Bousera peridotites (Internal Rif, Morocco) – Consequences for the Miocene evolution of the Gibraltar Arc. *Comptes Rendus l'Académie des Sciences* 321: 361–388.

Saji R, Chalouan A. 1995. Le bassin pliocène intramontagneux de Tirinesse et son mode d'ouverture (Rif interne, Maroc). *Geogaceta* 17: 110–112.

Sánchez-Rodríguez L, Gebauer D. 2000. Mesozoic formation of pyroxenites and gabbros in the Ronda area (southern Spain), followed by Early Miocene subduction metamorphism and emplacement into the middle crust: U-Pb sensitive high-resolution ion microprobe dating of zircon. *Tectonophysics* 316: 19–44. DOI: 10.1016/S0040-1951(99)00256-5.

Sanz de Galdeano C. 2019. Paleogeographic reconstruction of the Betic-Rif Internal Zone: an attempt. *Revista de la Sociedad Geológica de España* 32: 107–128.

Sanz de Galdeano C, Ruiz Cruz MDD. 2016. Late Palaeozoic to Triassic formations unconformably deposited over the Ronda peridotites (Betic Cordilleras): Evidence for their Variscan time of

crustal emplacement. *Estud. Geológicos* 72: e043. DOI: 10.3989/egeol.42046.368.

Serrano F, Guerra-Merchán A, El Kadiri K, *et al.* 2007. Tectono-sedimentary setting of the Oligocene-early Miocene deposits on the Betic-Rifian Internal Zone (Spain and Morocco). *Geobios* 40: 191–205. DOI: 10.1016/j.geobios.2006.04.005.

Serrano F, Sanz De Galdeano C, El Kadiri K, *et al.* 2006. Oligocene-early Miocene transgressive cover of the Betic-Rif Internal Zone. Revision of its geologic significance. *Eclogae Geologicae Helvetiae* 99: 237–253. DOI: 10.1007/s00015-006-1186-9.

Spakman W, Wortel R. 2004. A tomographic view on western Mediterranean geodynamics. In : Cavazza W, Roure FM, Spakman W, Stampfli GM, Ziegler PA, eds. *TRANSMED Atlas-The Mediterranean Region from Crust to Mantle Geological and Geophysical Framework of the Mediterranean and the Surrounding Areas*, pp. 31–52. DOI: 10.1007/978-3-642-18919-7_2.

Srivastava D, Lisle RJ, Vandycke S. 1995. Shear zones as a new type of palaeostress indicator. *Journal of Structural Geology* 17: 663–676.

Stampfli GM. 2000. Tethyan oceans. *Geological Society of London* Special Publications 173: 1–23.

Van Hinsbergen DJJ, Vissers RLM, Spakman W. 2014. Origin and consequences of western Mediterranean subduction, rollback, and slab segmentation. *Tectonics* 33: 393–419. DOI: 10.1002/2013TC003349.

Vazquez M, Jabaloy A, Barbero L, Stuart FM. 2011, Deciphering tectonic- and erosion-driven exhumation of the Nevado-Filábride Complex (Betic Cordillera, Southern Spain) by low temperature thermochronology. *Terra Nova* 23: 257–263. DOI: 10.1111/j.1365-3121.2011.01007.x.

Verges J, Fernandez M. 2012. Tethys-Atlantic interaction along the Iberia-Africa plate boundary: The Betic-Rif orogenic system. *Tectonophysics* 579: 144–172. DOI: 10.1016/j.tecto.2012.08.032.

Villaseñor A, Chevrot S, Harna M, *et al*. 2015. Subduction and volcanism in the Iberia – North Africa collision zone from tomographic images of the upper mantle. *Tectonophysics* 663: 238–249. DOI: 10.1016/j.tecto.2015.08.042.

Vitale S, Zaghloul MN, Tramparulo FDA, El Ouaragli B. 2014. Deformation characterization of a regional thrust zone in the northern Rif (Chefchaouen, Morocco). *Journal of Geodynamics* 77: 22–38.

Vitale S, Zaghloul MN, El Ouaragli B, Tramparulo FDA, Ciarcia S. 2015. Polyphase deformation of the Dorsale Calcaire Complex and the Maghrebian Flysch Basin Units in the Jebha area (Central Rif, Morocco): New insights into the Miocene tectonic evolution of the Central Rif belt. *Journal of Geodynamics* 90: 14–31. DOI: 10.1016/j.jog.2015.07.002.

Weijermars R, Roep TB, Van den Eeckhout B, Postma G, Kleverlaan K. 1985. Uplift history of a Betic fold nappe inferred from Neogene–Quaternary sedimentation and tectonics (in the Sierra Alhamilla and Almería, Sorbas and Tabernas Basins of the Betic Cordilleras, SE Spain). *Geologie en Mijnbouw* 64: 397–411.

Zeck HP, Albat F, Hansen BT, Torres-Roldán RL, Garciá-Casco A, Martín-Algarra A. 1989. A 21 ± 2 Ma age for the termination of the ductile alpine deformation in the internal zone of the betic cordilleras, South Spain. *Tectonophysics* 169: 215–220. DOI: 10.1016/0040-1951(89)90196-0.

Cite this article as: El Bakili A, Corsini M, Chalouan A, Münch P, Romagny A, Lardeaux JM, Azdimousa A. 2020. Neogene polyphase deformation related to the Alboran Basin evolution: new insights for the Beni Bousera massif (Internal Rif, Morocco), *BSGF - Earth Sciences Bulletin* 191: 10.